الجمـــهوريـــة الجـــزائريـــة الديـمقـراطيـــــــة الشـعبيـــــة
THE PEOPLE'S DEMOCRATIC REPUBLIC OF ALGERIA
وزارة التعـلـيـم الـعـالـــي و الـبـحـث الـعـلـمي
THE MINISTRY OF HIGHER EDUCATION AND SCIENTIFIC RESEARCH
جـامـعـة عمّـــار ثـلـيـــجـــي بالأغـــواط
AMAR TELIDJI UNIVERSITY OF LAGHOUAT
كـلـيـــــة الـتكنولوجيا
FACULTY OF TECHNOLOGY
قسم الالكترونيك
DEPARTMENT OF ELECTRONIC

Master's dissertation

Domain: Science and Technology

Field: Electronic

Option: Instrumentation

Submitted By: **MERAD HADIL**

THEME

MATLAB/Simulink Medical CO2 insufflator model with PID

Jury members:

M^{me}. DJERFAF FATIMA	***Pr.***	***Examinator***	***UATL***
Mr. MECHRI KIOUS	***Pr.***	***President***	***UATL***
M^{me} . Leila Amal Vilbois	***MAA.***	***Supervisor***	***UATL***

Academic year 2024/2025

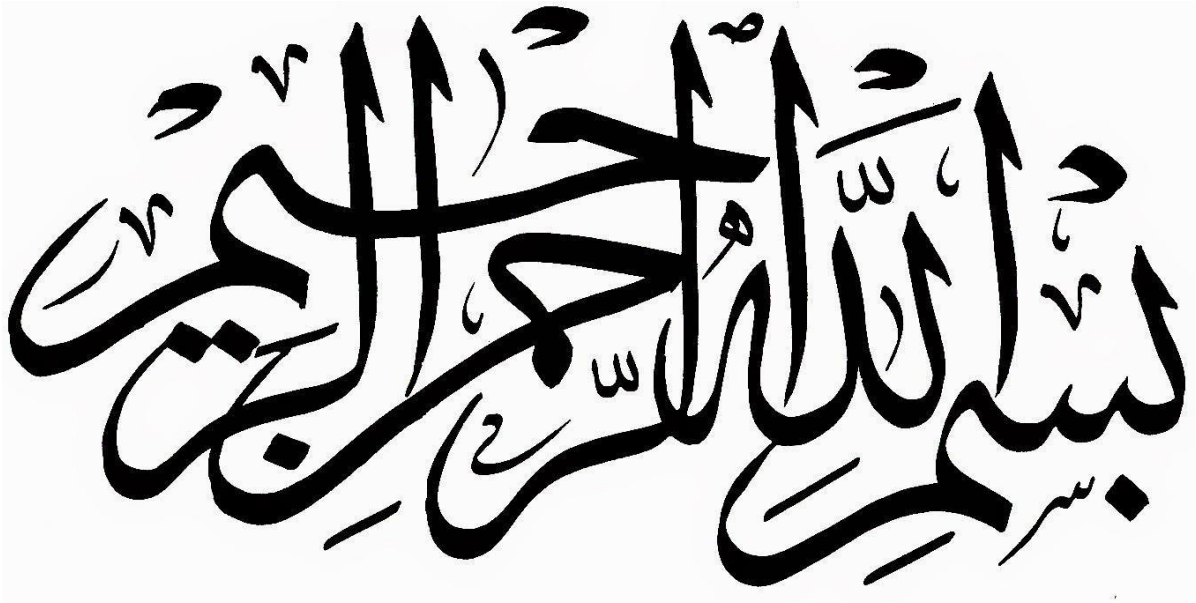
بسم الله الرحمن الرحيم

Acknowledgments

First and foremost, I am deeply thankful to God for granting me the strength, health, and perseverance needed to bring this work to completion.

I would like to express my sincere appreciation to my supervisor, Mme. Leila Amal Vilbois, for her ongoing support, wise counsel, and invaluable guidance throughout this project. Her encouragement has been a driving force and a true source of inspiration. It has been a privilege to carry out this work under her supervision.

I am also grateful to all the faculty members and administrative staff of the Electronics Department at Amar Telidji University of Laghouat

Lastly, I extend my heartfelt thanks to the members of the jury who will evaluate this project. I truly value their time, insights, and constructive feedback. I also wish to thank everyone who, in one way or another, helped and supported me during the course of this project.

Thankyou all…

Dedicate

To the source whose giving never fades,
to the one who wove my happiness from the pure threads of her heart...
To my beloved mother.
To the one who toiled and stayed up countless nights so I could live in peace and comfort,
to the one who spared no effort to support me on the path to success,
to the one who taught me to face life with wisdom and resilience...
To my dear father.
To those whose love flows in my veins and whose memory brings warmth to my soul...
To my cherished sister and siblings.
And to everyone who believed in me and stood by my side so I could fulfill my academic dream...

HADIL

Contents

Chapter II: CO_2 Insufflation and PID-Based Pressure Control in Medical Devices.

Chapter III:PID Pressure Control Modeling in MATLAB/Simulink

List of abbreviations

Bar: the unit of pressure in bar.

C°: degree Celsius temperature unit.

GA: General anaesthesia.

Hypercarbia: increased carbon dioxide levels.

IAP: Intra-Abdominal Pressure.

IVC: Compression of the Inferior vena Cava.

K: kelvin temperature unit.

LOW: Low pressure unit.

MAP: mean arterial pressure.

MIS: Minimally invasive surgery.

mmHg: millimeter of mercury unit of pressure.

P: Pressure.

Pa: the unit of pressure in pascal.

PAP: Pulmonary Artery Pressure.

PID: Proportional-Integral-Derivative.

PPR: Proportional pressure regulator.

RAP: Right Atrial Pressure.

SA: Spinal Anaesthesia.

SVR: systemic vascular resistance.

T: Temperature.

TEE: Transesophageal Echocardiography.

List of figures

List of tables

General introduction

Laparoscopic Minimally Invasive Surgery (MIS) relies on the use of a medical CO_2 insufflator to create and maintain pneumoperitoneum by expanding the abdominal cavity. To ensure patient safety during this procedure, it is essential to monitor and control the pressure and temperature of the incoming CO_2 gas with high precision.

To achieve this, a pressure control system has been designed using a Proportional-Integral-Derivative (PID) controller to regulate a Proportional Pressure Regulator (PPR) integrated into the pneumatic system. Additionally, a nonlinear model of the abdominal cavity has been developed to analyze the dynamic behavior of the insufflation process. The integration and simulation of all system components into a single model have shown promising results [1]. The objective of this work is to further evaluate the performance of this system and validate the simulation results. This project is structured into three chapters:

- **Chapter 1** presents a literature review and an overview of CO**2** insufflation in medical procedures. Through this chapter, we explore the medical context, understand the fundamental purpose of insufflation, and acquire relevant terminology and background knowledge. It also introduces the basic concepts of electronics and PID controllers as used in medical devices.
- **Chapter 2** dives deeper into both medical and engineering aspects. On the medical side, it discusses the principles of CO_2 insufflation and the importance of pressure regulation in surgical applications. On the technical side, it covers PID control theory and its relevance to medical instrumentation.
- **Chapter 3** focuses on the practical implementation and simulation. It presents the complete development of a medical CO_2 insufflator model using MATLAB/Simulink with Simscape (2019). This computational model incorporates sensors (pressure, temperature, etc.) and actuators (solenoid valves, pressure-reducing valves, safety valves, etc.). A PID controller has also been implemented to accurately drive the Proportional Pressure Regulator (PPR) within the pneumatic system.

This structured approach enables a comprehensive understanding of both the medical context and the engineering methods used to model and control the CO_2 insufflation process in laparoscopic surgery.

Chapter I

CO_2 Insufflation and PID Control in Medical Procedures

I.1 Introduction

Laparoscopy involves examining the abdominal cavity by inserting a tube through the abdominal wall, using gas to expand the cavity, and viewing the contents with a lighted scope [2]. Recently, minimally invasive surgery has become common, but laparotomy is still performed based on the patient's condition. After open surgery, typical complications include post-operative ileus, infection, and wound issues [3]. In high-risk patients, laparoscopic surgery is often preferred, yet common risk assessment tools lack validation for this method. Newer risk scores have been studied but do not focus specifically on laparoscopic patients. Laparoscopic surgery generally has a lower cardiovascular mortality risk, and understanding its specific risks is important for patient safety [4].

I.2 Phases of laparoscopic surgery

Laparoscopic surgery consists of 4 phases: induction of anesthesia, abdominal insufflation, abdominal desufflation, and recovery from anesthesia. Each phase has unique hemodynamic and ventilatory changes. (Cardiovascular and Ventilatory Consequences of Laparoscopic Surgery) [4].

Figure I.1: laparoscopic surgery [5].

I.2.1 Induction of anesthesia

All laparoscopic abdominal surgery patients offered SA as first choice,4645 consecutive patients have undergone laparoscopic abdominal surgery under SA since 1995.Patients who preferred GA or who had a contraindication to the SA, such as children under the age of 10, patients with coagulation disorders, spinal deformities and skin pathology overlying the SA site underwent surgery under GA and were retained as controls [6]. Choosing an anesthetic depends on the type of surgery and patient characteristics, The objectives of laparoscopic surgery in the day case setting, which is predominantly gynecological, are as follows, The aim is to achieve a rapid recovery with minimal residual effects, good control of pain and freedom from nausea and vomiting [7].

I.2.2 Abdominal insufflation (Pneumoperitoneum)

Laparoscopic surgery starts by inserting a Veress needle or trocar into the abdominal cavity, followed by the introduction of carbon dioxide (CO_2) to establish an intra-abdominal pressure (IAP) ranging from 12-15 mmHg.CO_2 is the preferred gas for insufflation because:

- It has minimal flammability risks
- Its high solubility in blood lowers the chances of a gas embolism (0.0014%-0.6%)
- It helps maintain warmth within the abdominal cavity by creating a thermal insulation effect [4].

I.2.2.1 Potential Risks Associated with Trocar Insertion and CO_2 Insufflation

If the trocar punctures a major blood vessel, it may cause severe bleeding and CO_2 embolism, which can lead to cardiovascular collapse.

Transesophageal echocardiography (TEE) is useful for detecting gas embolism stages by monitoring right heart chamber filling. To manage CO_2 gas embolism:

- Stop CO_2 insufflation immediately

- Position the patient in a left lateral decubitus position

-Administer100%oxyge(FiO2 100%) [4].

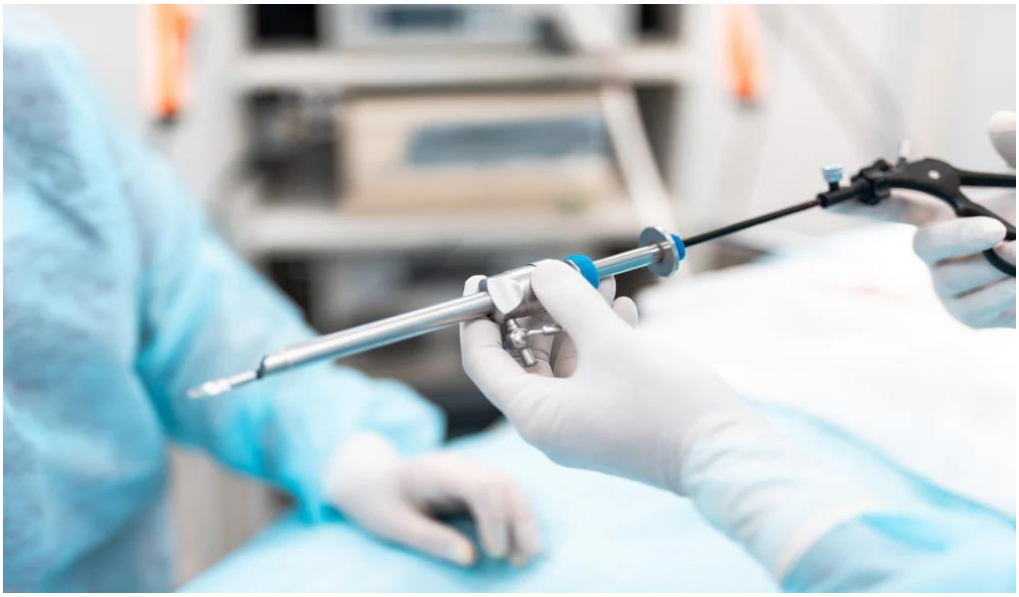

Figure I.2: Trocar [8].

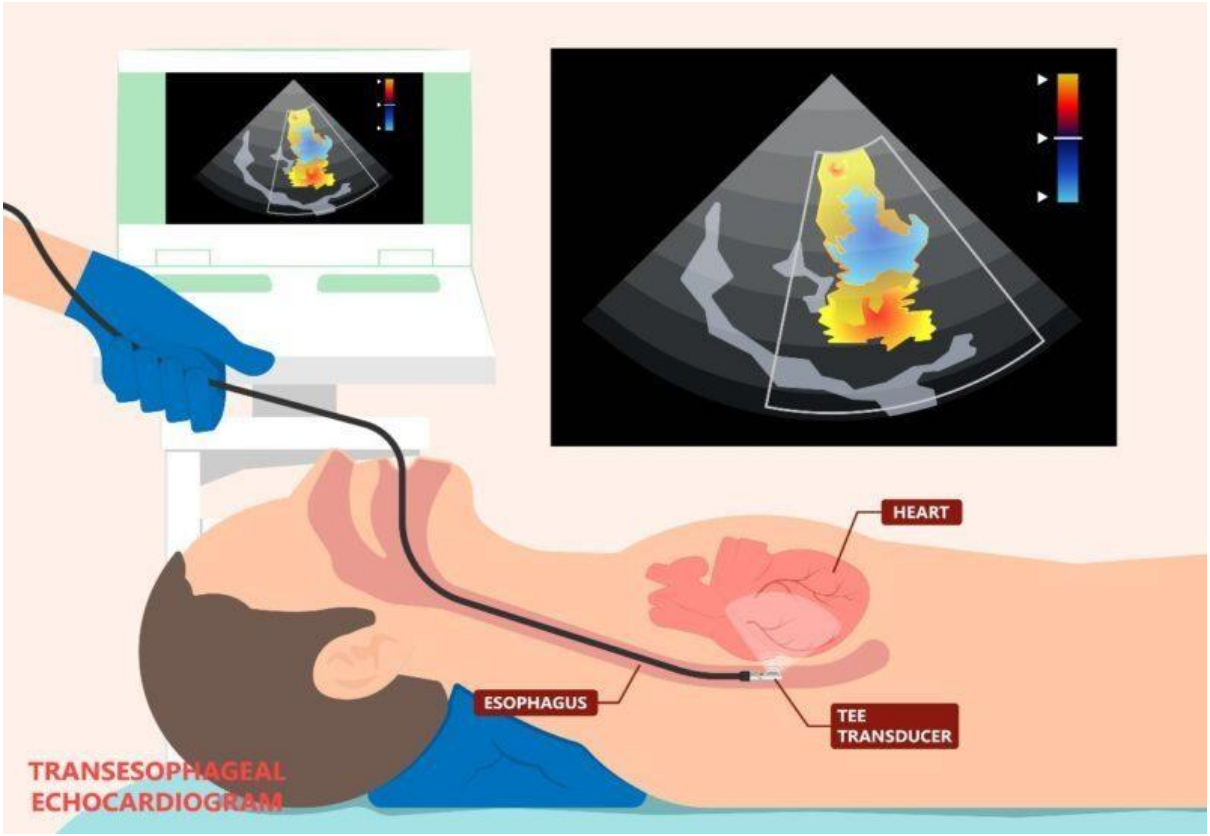

Figure I.3: Transesophageal Echocardiography TEE [9].

I.2.2.2 Physiological Consequences of CO_2 Insufflation

Elevated IAP and hypercapnia (excess CO_2 in the blood) impact:

- Cardiac function

- Pulmonary mechanics

- Renal circulation

Studies conducted on both humans and animals suggest that the hemodynamic effects of increased IAP result from a combination of mechanical forces and neurohormonal responses, leading to:

1. Compression of the inferior vena cava (IVC)
2. Constriction of the aorta
3. Reduced blood supply to abdominal organs (splanchnic circulation)
4. Decreased kidney perfusion
5. Diaphragmatic elevation, which affects breathing [4].

I.2.2.3 How Increased Abdominal Pressure Impacts Circulation and the Heart

IVC compression alters venous return dynamics and venous resistance.

- In animal studies, IVC pressure rises with higher IAP, initially leading to an increase in right atrial pressure (RAP) until IAP reaches 15 mmHg.

- At low IAP values (5 mmHg), a brief rise in cardiac output (CO) occurs as compressed blood from the abdominal organs is redirected toward the heart.

- As IAP continues to rise, venous return and cardiac output progressively decline due to restricted blood flow in the IVC, causing blood pooling in the lower limbs.

- Blood supply to the liver (hepatic arterial and portal circulation) diminishes, reducing visceral oxygenation while shifting circulation toward the central cardiovascular system, leading to sustained elevation of right atrial pressure [4].

I.2.2.4 Effects of Increased Abdominal Pressure on Blood Circulation and vascular resistance

Pneumoperitoneum elevates mean arterial pressure (MAP) and systemic vascular resistance (SVR), which can compromise cardiac output (CO).

Studies in healthy individuals demonstrated a rapid increase in SVR and MAP within the first five minutes of insufflation due to aortic compression and autonomic nervous system responses [4].

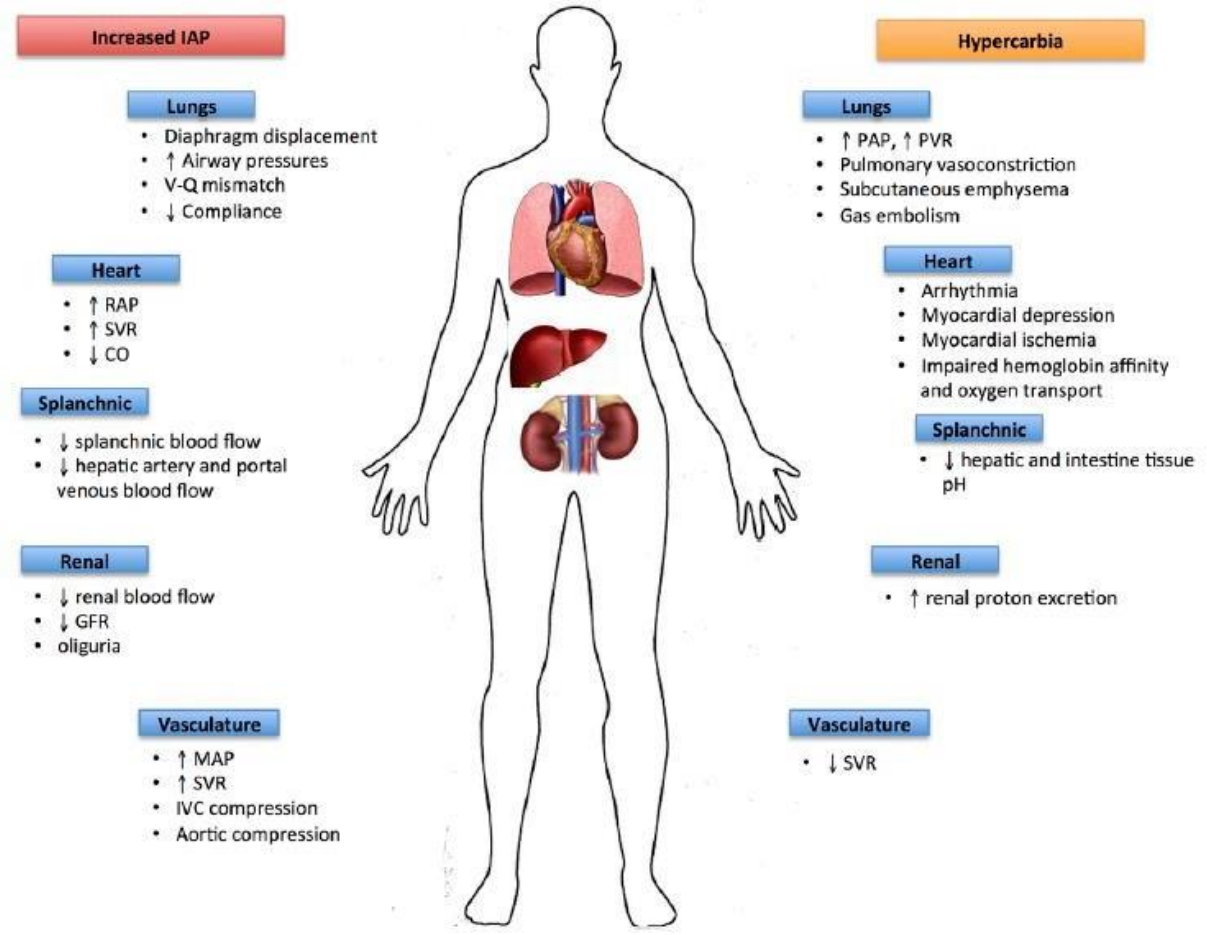

Figure I.4: Two components of laparoscopic surgery [4].

The negative effects of high intra-abdominal pressure (IAP) and increased carbon dioxide levels (hypercarbia) are detailed. Key terms include cardiac output (CO), glomerular filtration rate (GFR), intra-abdominal pressure (IAP), mean arterial pressure (MAP), pulmonary artery pressure (PAP), right atrial pressure (RAP), and systemic vascular resistance (SVR).

Research indicates that rising plasma levels of norepinephrine, epinephrine, cortisol, vasopressin, atrial natriuretic peptide, renin, and aldosterone occur with decreasing renal blood flow due to IAP compression, which lowers CO and triggers renin release. At IAP levels of7. 5 mm Hg, both RAP and CO increase, but at 15 mm Hg and above, CO decreases. Transesophageal echocardiography (TEE) shows rapid cardiovascular changes during laparoscopic procedures, with parameters often returning to normal within 30 minutes. Pneumoperitoneum can harm kidney function, potentially leading to acute kidney injury, especially in those with chronic kidney disease [4].

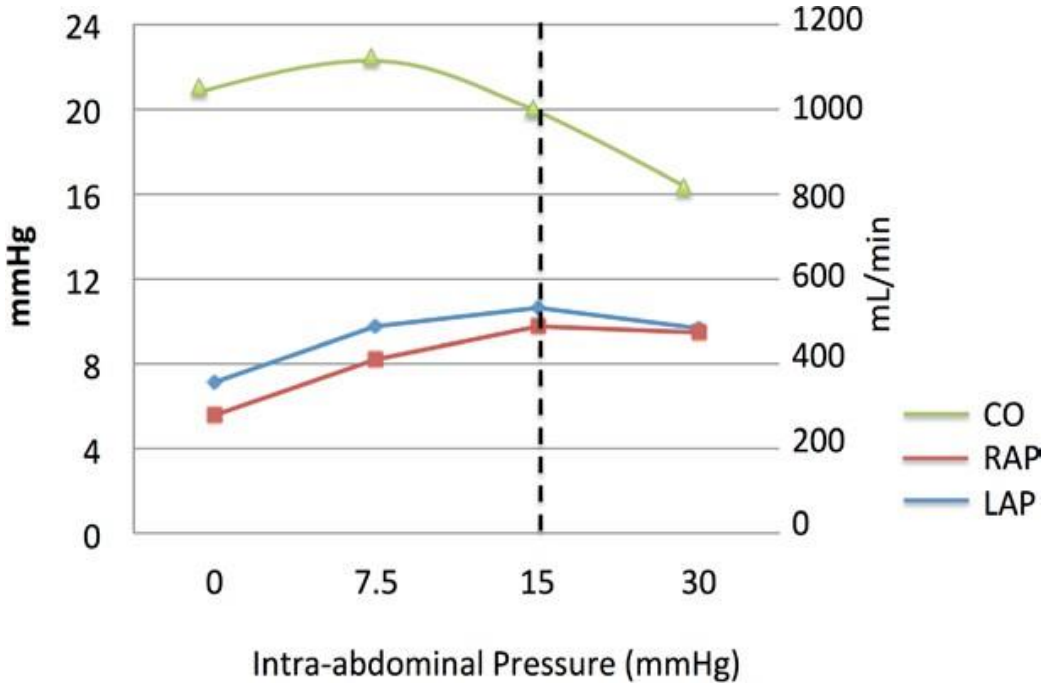

Figure I.5: Hemodynamic effects of IAP [4].

I.2.2.5 Effects of Abdominal Insufflation on Pulmonary Function

Abdominal insufflation has notable effects on respiratory function. As intra-abdominal pressure (IAP) rises, the diaphragm shifts upward, a displacement that becomes more pronounced in the Trendelenburg position. This cephalad movement of the diaphragm, combined with the need for increased minute ventilation, leads to higher airway pressures. Studies have shown that pulmonary compliance decreases under these conditions, accompanied by elevated peak and plateau airway pressures and a reduction in functional residual capacity. These factors can contribute to ventilation-perfusion imbalances, increasing the risk of hypoxemia.

The insufflation gas, carbon dioxide (CO_2), diffuses into the bloodstream, causing an elevation in the partial pressure of CO_2 within minutes of the procedure. To maintain normal CO_2 levels, an increased respiratory rate is often necessary. If end-tidal CO_2 ($ETCO_2$) continues to rise beyond 30 minutes, subcutaneous emphysema should be considered as a possible cause.

Subcutaneous emphysema, which results from CO_2 leaking into subcutaneous tissues, occurs in 0.43% to 2.3% of cases and can contribute to hypercapnia and metabolic acidosis.

Several factors increase the risk of developing subcutaneous emphysema, including prolonged surgical duration (>3.5 hours), IAP levels exceeding 15 mm Hg, incorrect cannula placement outside the peritoneal cavity, fascial disruptions, $ETCO_2$ levels above 50 mm Hg, the use of multiple cannulas (>5), and high gas flow rates. To reduce CO_2 leakage, surgical techniques such as securing Hasson ports and minimizing tissue extraction through port sites are recommended. Treatment involves increasing ventilation, and if this proves insufficient, deflating the abdomen may be necessary [4].

I.2.2.6 Major Pulmonary Complications of Abdominal Insufflation

There are four primary pulmonary complications associated with abdominal insufflation:

1. Hypercapnia: Excess CO_2 can lead to systemic vasodilation, arrhythmias, myocardial depression, and worsening pulmonary hypertension. To counteract this, increased ventilation is required to facilitate CO_2 removal.
2. Hypoxemia: Reduced lung compliance and ventilation-perfusion mismatch can lower oxygen levels in the blood.
3. Decreased Pulmonary Compliance: The increased airway pressures and diaphragm displacement reduce the lungs' ability to expand efficiently.
4. Subcutaneous Emphysema : CO_2 accumulation in subcutaneous tissues can exacerbate respiratory complications and acid-base imbalances[4].

I.2.2.7 Cardiovascular Effects and bradyarrhythmias

The stretching of the peritoneum during insufflation can activate the vagus nerve, leading to bradyarrhythmias and, in severe cases, asystole. The incidence of bradyarrhythmias is estimated to be 14–27% in young, healthy individuals. Patients on β-blockers may be at an even higher risk due to reduced compensatory responses.

To minimize vagally induced bradycardia, surgeons can adopt strategies such as gradual insufflation, using lower IAP levels, and administering preoperative glycopyrrolate. If bradycardia develops, immediate intervention is crucial. This includes reducing IAP by opening the ports, administering a fluid bolus, and coordinating with the anesthesiologist to adjust the procedure. If necessary, reattempting insufflation with a lower IAP is often safe. However, if a patient cannot tolerate pneumoperitoneum, conversion to an open surgical approach may be required. Prompt recognition and management of bradycardia are essential, as it can sometimes be an early warning sign of cardiac arrest, though such cases are rare [4].

I.2.3 Abdominal desufflation and recovery

Final stages of anesthesia involve desufflation, which is the release of CO_2 from the abdomen, followed by the recovery phase. Even after desufflation, the body may still retain up to 120 liters of CO_2, requiring sustained increased ventilation for effective elimination. CO_2 is primarily removed through the lungs and renal proton excretion.

In cases of significant hypercapnia, the anesthesiologist must carefully determine the ideal timing for extubation to ensure sufficient CO_2 clearance. If CO_2 removal is incomplete, it can contribute to considerable postoperative discomfort, sometimes manifesting as referred pain in the left shoulder, which may be mistaken for cardiac-related chest pain.

In healthy individuals, hemodynamic parameters typically normalize immediately after desufflation. However, in patients with pre-existing cardiovascular conditions, these changes may persist for over an hour. In elderly individuals with heart disease, desufflation has been linked to increased heart rate, enhanced cardiac index, elevated left ventricular stroke work index, improved ejection fraction, and a reduction in systemic vascular resistance (SVR).

Among cardiovascular patients undergoing laparoscopic surgery, 20% developed heart failure within the first three hours postoperatively. Those affected experienced a marked decline in cardiac index (down to 65% of baseline), left ventricular stroke work, and stroke volume. As a result, careful monitoring for signs of myocardial ischemia and heart failure in the immediate postoperative period is crucial to ensure timely intervention if complications arise[4].

I.3 Challenges of abdominal access in laparoscopy

One of the key challenges in laparoscopic surgery is gaining access to the abdominal cavity, as it requires inserting surgical instruments through small incisions. This process carries a risk of injury to major blood vessels and the gastrointestinal tract, with over half of such serious complications occurring before the actual procedure even begins.

Despite advancements in surgical techniques, the rate of these complications has remained largely unchanged over the past 25 years. Most injuries occur during the placement of the primary umbilical trocar. If these injuries go unnoticed or are not addressed promptly, they can lead to significant increases in morbidity and mortality.

To reduce the risk of access-related injuries, various techniques, specialized instruments, and alternative approaches have been developed and refined over the years [2].

I.4 Techniques for abdominal entry in laparoscopy

Several techniques have been developed to facilitate safe abdominal access in laparoscopic surgery. These include the Veress needle with pneumoperitoneum followed by trocar insertion (also known as the closed-entry or "classic" technique), the open (Hasson) method, direct trocar insertion without prior insufflation, shielded disposable trocars, optical Veress needles, optical trocars, radially expanding trocars, and trocar less reusable visual access cannulas. The choice of entry technique often depends on the surgeon’s level of training, personal experience, and preference, as well as regional surgical practices and interdisciplinary differences. This guideline evaluates the current evidence supporting various laparoscopic entry methods and offers recommendations based on the standards set by the Canadian Task Force on Preventive Health Care [2].

I.4.1 Closed entry (classic) laparoscopy

The traditional closed-entry laparoscopic approach involves making an incision in the abdominal skin with a scalpel, followed by insufflation of air or gas to create pneumoperitoneum. A sharp trocar and cannula system are then introduced into the abdominal cavity. Once the trocar is withdrawn, an illuminated telescope is inserted through the cannula, allowing for visualization and examination of the abdominal cavity[2].

I.4.1.1 Establishment of pneumoperitoneum, the veress needle

In 1947, Raoul Palmer from France played a key role in popularizing the use of the Veress needle for inducing pneumoperitoneum with CO_2 in laparoscopy. He later documented its safety in his first 250 patients. Palmer highlighted that the creation of pneumoperitoneum is a crucial initial step, though it remains associated with potential complications. Studies suggest that the majority of gynecologists performing laparoscopy globally rely on the Veress needle technique combined with a primary trocar for abdominal access. A Canadian survey of 407 obstetricians and gynecologists (51% response rate) revealed that 96.3% consistently establish

pneumoperitoneum before inserting the primary trocar, while 1.2% do so occasionally, and 2% never (0.5% did not respond). Additionally, 26.4% of respondents reported encountering vessel or organ injuries linked to the Veress needle, whereas injuries from the primary and secondary trocars were reported by 25.6% and 15.0%, respectively [2].

I.4.1.2 Veress Needle Insertion Sites

Typically, the Veress needle is introduced in the umbilical region along the midsagittal plane, with or without manually elevating the anterior abdominal wall for stabilization. However, in cases where periumbilical adhesions are suspected or when three consecutive attempts to establish pneumoperitoneum fail, alternative insertion sites should be considered [2].

I.4.1.3 CO_2 Insufflation via Left Upper Quadrant (LUQ) – Palmer's Point

For patients with a history of laparotomy, Palmer recommended inserting the Veress needle approximately 3 cm below the left subcostal margin along the midclavicular line.

This approach is particularly useful in both very thin and obese individuals. In lean patients with a pronounced sacral promontory or android pelvis, major blood vessels can be positioned just 1–2 cm beneath the umbilicus. Conversely, in obese women, the umbilicus may shift downward toward the aortic bifurcation [2].

LUQ insufflation requires prior gastric decompression using a nasogastric tube and inserting the Veress needle at a perpendicular angle to the skin. Patients with prior gastric or splenic surgery, significant hepatosplenomegaly, portal hypertension, or gastropancreatic tumors should be excluded from this method. Compared to the umbilical region, the LUQ site has less subcutaneous fat. Research by Tulikangas et al. demonstrated a correlation between BMI and the distance between intra-abdominal structures and insertion points.

Once pneumoperitoneum is successfully established, trocars of different sizes and designs may be introduced at the same site as the Veress needle, with additional trocar or cannula systems placed under direct visualization as necessary [2]

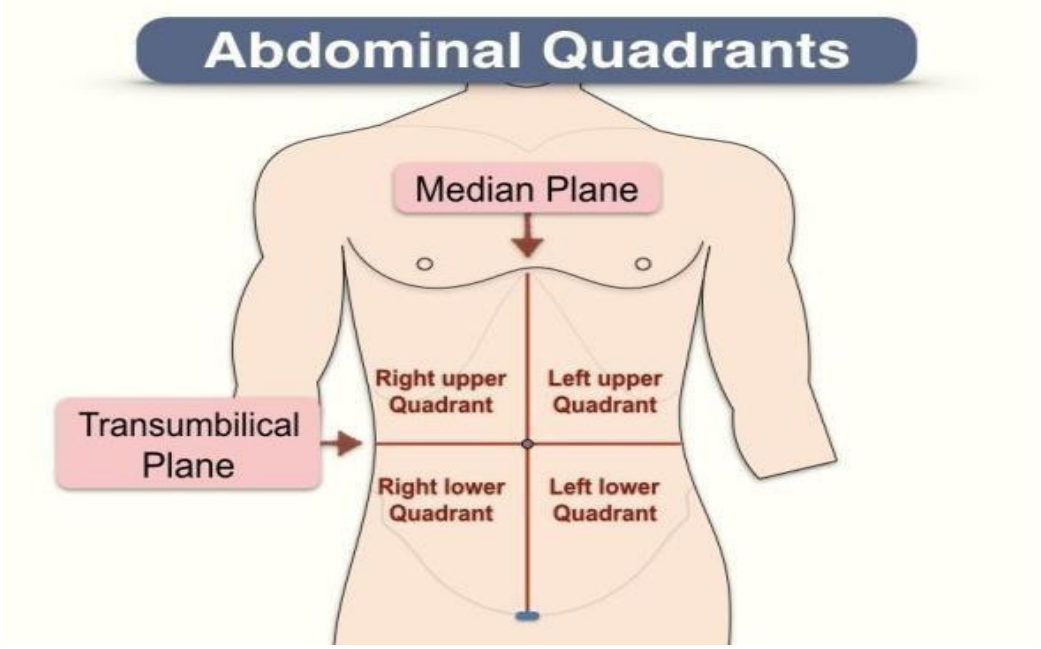

Figure I.6: Abdominal Quadrants [10].

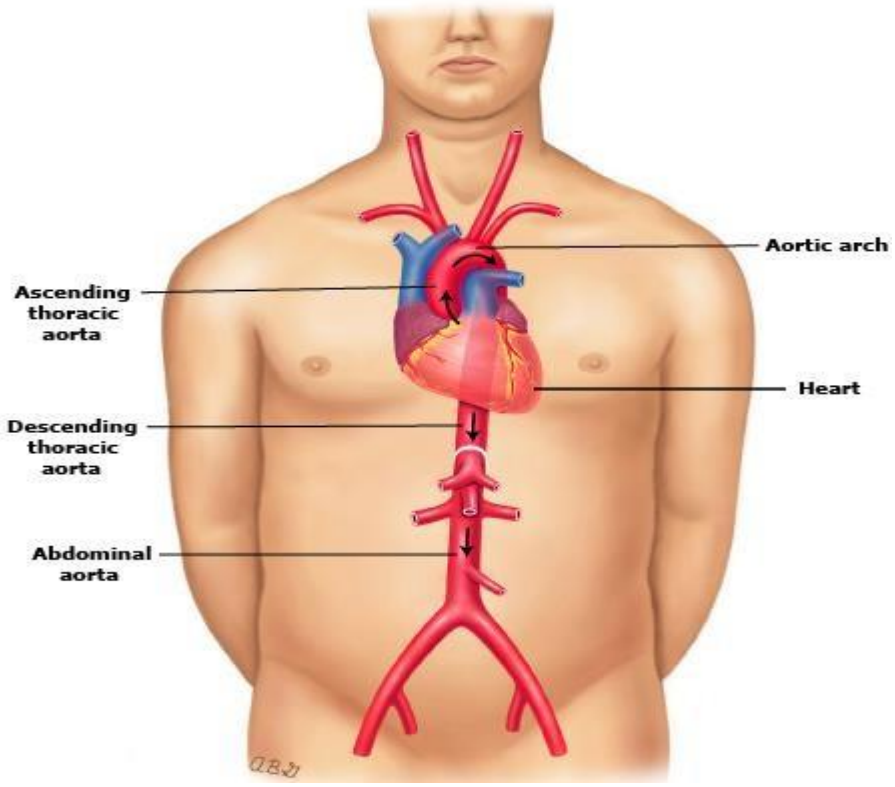

Figure I.7: aortic bifurcation [11].

I.4.1.4 Number of Veress Needle Insertion Attempts

Research indicates that successful placement of the Veress needle into the peritoneal cavity on the first attempt occurs in approximately 85.5% to 86.9% of cases. In 8.5% to 11.6% of procedures, a second attempt is necessary, while a third attempt is required in 2.6% to 3.0% of cases. More than three attempts are needed in only 0.3% to 1.6% of cases.

The risk of complications increases with the number of attempts. When the needle is inserted successfully on the first try, complication rates range from 0.8% to 16.3%. For those requiring a second attempt, complications occur in 16.31% to 37.5% of cases. When three attempts are necessary, the risk rises to 44.4% to 64%, and for more than three attempts, complications are reported in 84.6% to 100% of cases. Identified complications include extraperitoneal insufflation, bowel and omental injuries, and unsuccessful laparoscopy [2].

I.4.2 Open laparoscopic entry or Hasson technique

The open entry technique, introduced by Hasson in 1971, offers many benefits, such as a lower chance of gas embolism and fewer serious injuries.

The method uses a special cannula with a cone-shaped sleeve and a blunt obturator, and sometimes an extra sleeve for stay sutures. The process starts with a small cut at the umbilicus, allowing access to the peritoneal cavity. A blunt obturator helps insert the cannula, and sutures are applied to seal the area around it. Once the laparoscope is inserted, insufflation occurs. After the procedure, the fascia is sewn shut, and the skin is realigned. Hasson reviewed studies comparing open and closed laparoscopy techniques and found lower complication rates with open laparoscopy, such as 0. 4% for umbilical infections and 0. 1 % for bowel injuries. He suggested that the open technique is the better choice, as general surgeons had more complications with closed techniques than gynecologists. In his own experience, he reported only one bowel injury among 5,284 cases[2].

I.5 PID controllers in medical devices:

The PID controller has a long history in automatic control, starting in 1769 when James Watt developed a steam engine with a governor, the first negative feedback device. In 1868, J. C. Maxwell created a mathematical model for the governor control and classified governors into moderators (only proportional control) and genuine governors (proportional and integral actions). Nicolas Minorsky later analyzed the error derivative, which contributed to modern.

PID controllers despite initial resistance. In 1911, Elmer Sperry designed the first PID controller for the US Navy. By 1939, Taylor Instrument Companies improved their "Fulscope" pneumatic controller with a "pre-act" function, while Foxboro introduced "Stabilog" with "Hyper-reset. " Both innovations factored in the error signal's derivative, promoting PID control adoption. The issue of steady-state error was addressed through a proportional-integral (PI) controller approach. In 1940, Taylor developed a pneumatic controller with derivative action to reduce overshoot, and in 1942, Ziegler and Nichols introduced tuning rules for optimal PID parameters. By the mid-1950s, PID controllers were standard in industries.

Research continues to enhance PID tuning methods and control strategies. PID control relies on proportional, integral, and derivative components to adjust control output, making it widely used in various industries, including modern applications like self-driving cars and

robots. It is estimated that 90–95% of control loops in industrial systems depend on PID controllers[12].

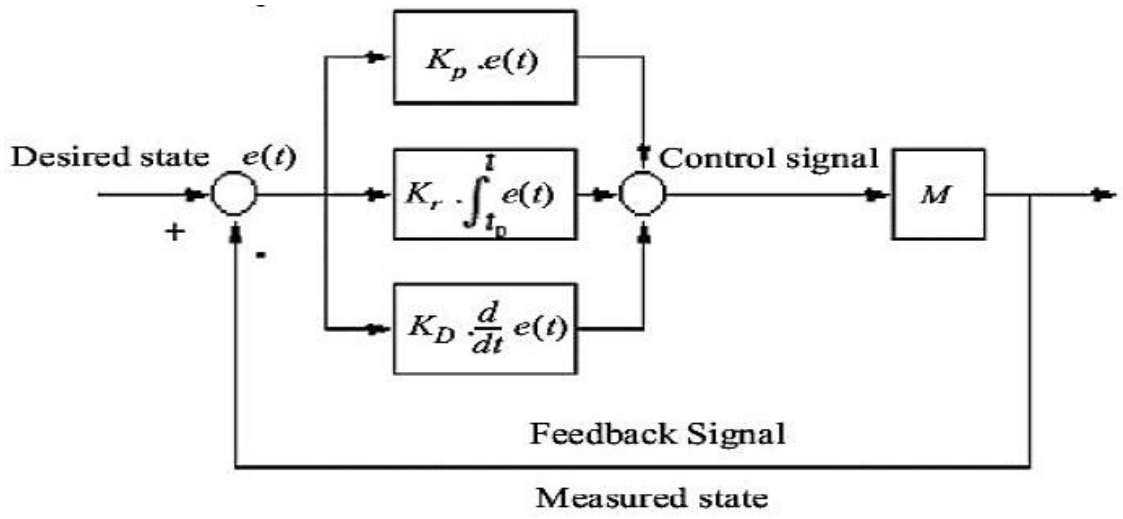

Figure I.8: A schematic representation of industrial regulation with PID [13].

I.6 Design and adjustment methodologies of PID Control Systems:

I.6.1 Configurations of PID controllers with parameters:

The most commonly used topologies for PID devices are the series and parallel configurations [13].

- **Parallel Configuration**: In this structure, the proportional (P), integral (I), and derivative (D) actions function independently in separate solution components, and the overall response is obtained by combining the effects of all three actions. Each parameter operates independently

without influencing the others, and the corresponding control equation is represented as follows [13].

$$U_t = K_p \times e_t + K_i \int e_t \times dt + K_p \times \frac{de}{dt} \quad \text{(I.1)}$$

A PID controller processes the corresponding error signal (e) and determines its derivative as well as its accumulated sum over time. This error signal is then fed into the controller.

The resulting control signal (u), which is sent to the system, consists of three key components: the proportional gain (K_p) multiplied by the magnitude of the error, the integral gain (K_i) applied to the integral of the error, and the derivative gain (K_D) multiplied by the rate of change of the error [13].

- **Series Configuration:** The series formulation, also known as the cascaded formula, is primarily based on the characteristics of hydraulic and analog electrical circuits. Unlike an ideal PID formulation, adjustments in this configuration influence all three control actions. However, the proportional action is specifically affected by both the integral and derivative components. The structural difference between the series and parallel configurations is illustrated in Figure 2 (a) and (b), respectively [13].

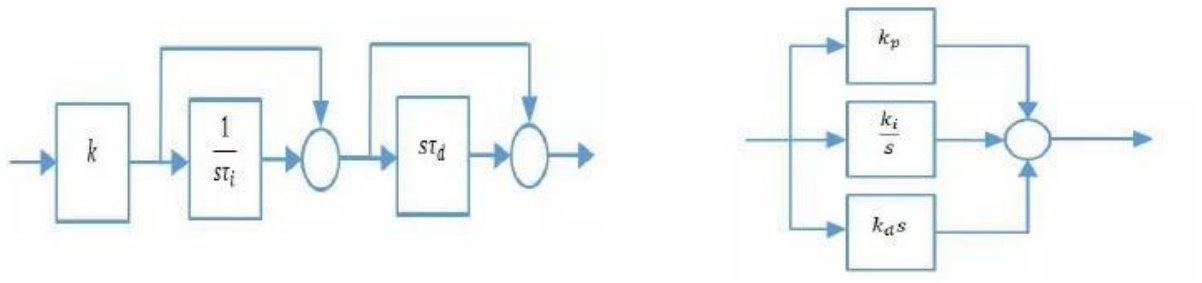

Figure I.9: Configuration of PID (**a**) Series Type (b) Parallel Type [12].

I.7 PID for biomedical applications

Various PID-based control strategies have been explored for biomedical applications, including the regulation of arterial blood pressure, muscle relaxation during surgery, joint angle control in artificially stimulated muscles, liver transplantation, blood glucose management, and the administration of propofol anesthesia. In, Slate and Sheppard implemented a nonlinear digital PID controller to regulate arterial blood pressure by administering sodium nitroprusside. This method is particularly used in cardiac surgical intensive care units during open-heart surgery to manage hypertension. In, Satoru Isaka and Anthony V. Sebald examined the use of automatic control techniques for arterial blood pressure regulation.

Their study included a variety of approaches, such as PID control and its modifications, optimal control, adaptive control, rule-based control (including fuzzy logic control), and neural network-based control methods. Denai et al. developed a self-tuning PID system to regulate muscle relaxation induced by atracurium in surgical patients. Additionally, Veltink et al. introduced a control system for joint angle regulation in artificially stimulated muscles. Advanced PID control methods have also been proposed for blood glucose regulation, including expert PID control and improved PID switching strategies. Furthermore, O'Hara et al. utilized a PID controller to model the pharmacokinetics and pharmacodynamics of vecuronium during liver transplantation. In a separate study, Van Heusden et al. introduced a robust PID control approach to regulate propofol anesthesia in pediatric patients [12].

I.8 Conclusion

We have explored in this chapter the initial literature review on laparoscopic surgery, its techniques, and CO_2 insufflation methods while considering internal abdominal factors such as temperature and pressure. Additionally, we have defined the PID controller and its various types. Building on this foundation, we will now delve deeper into the fundamentals of CO_2 insufflation and the methods used to regulate the pressure of medical instruments.

Chapter II

CO2 Insufflation and PID-Based Pressure Control in Medical Devices.

II.1 Introduction

Laparoscopy may be considered one of the greatest advances in surgery. It has revolutionized how we use digital and robotic technology to practice surgery. compared to 'open' surgery it has radically reduced patient recovery time [14]. To create and maintain this condition, insufflators are used. Insufflators are medical devices for the regulation of pressure and flow of a gas supply during laparoscopic surgery. To inflate the peritoneal cavity from a high-pressure medical gas tank (e.g. CO2, N2O). This leads to a huge workspace. many types of actuators and control systems are required to control and operate insufflators in today's rapidly growing technology. Two sources, electrical and pneumatic, are important for the operation of medical insufflators [1].

II.2 Principal of CO2 insufflation

II.2.1 Creation of pneumoperitoneum

The knowledge of the basic physiological mechanisms altered by laparoscopy and pneumoperitoneum is essential [15].

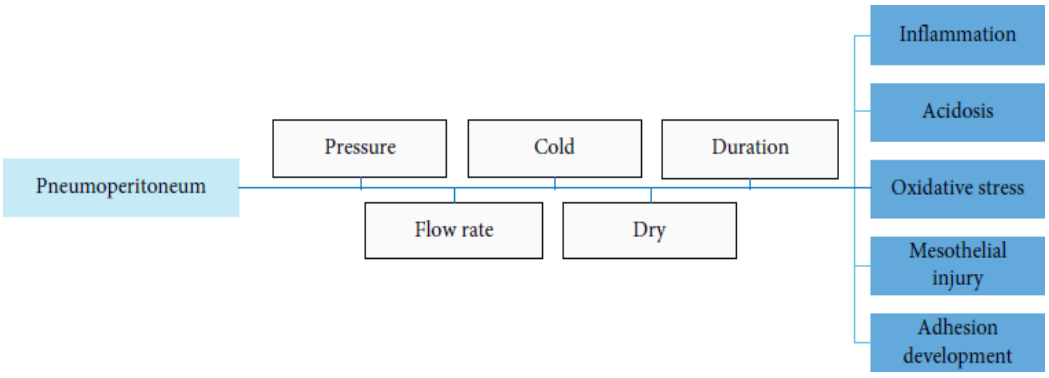

Figure II.1: Pneumoperitoneum characteristics and related peritoneal effects [15].

II.2.2 physiological properties of CO2

Carbon dioxide (CO_2) is widely used for insufflation in laparoscopic surgery. It is non-combustible, inexpensive, and easily absorbed and eliminated [16].

$CO2+H2O \rightarrow H2CO3 \rightarrow H^+ + HCO3$ [16]

II.2.3 pressure regulation

- Phase 1: when IAP reached 5 mmHg from baseline.
- Phase 2: when IAP had increased from 5 mmHg to 10 mmHg.

- Phase 3: when IAP increased from 10 mmHg to 15 mmHg.

The CO2 volumes insufflated to achieve an intraabdominal pressure of 5 mmHg (IAV1),10 mmHg (IAV2), and 15 mmHg (IAV3) were recorded (Figure II.2) [17].

II.2.4 Minimizing tissue damage

Open abdominal surgery can lead to complications such as postoperative ileus, infection, and bowel obstruction, partly due to exposure of the intestines to cold, dry air in the operating room. humidified carbon dioxide (CO_2) has been proposed. Because CO_2 is heavier than air, it settles in the abdominal cavity, creating a greenhouse effect that helps retain warmth and moisture [18].

II.2.5 Enhanced visualization

Surgeons have always wanted to use preoperative imaging to guide them during surgery. Modern tools now help make that possible, especially in laparoscopic surgery, which uses cameras instead of direct vision. These tools include:

- Augmented Reality (AR): overlays CT/MRI scans on live camera views to help guide surgeons.
- Fluorescence Imaging: uses special dyes like ICG to highlight blood flow, bile ducts, or tumors.
- 3D and HD Laparoscopes: improve depth perception and image clarity.
- New technologies like microscopic imaging may soon help detect cancer cells during surgery.

Some tools like ICG and 3D cameras are already in use, while others like AR and targeted dyes are still being developed. all of these aim to make surgery safer, faster, and more accurate [19].

II.3 Types of Laparoscopic Insufflation

Laparoscopic insufflators can be divided into two types: pneumatic insufflators and electronic insufflators. In the case of the pneumatic type, the gas is continuously injected into the peritoneal cavity until the pressure in the abdomen reaches the set value. the electronic insufflator, on the other hand, introduces the gas only during the insufflation phase, and then measures the pressure in the zero flow measurement phase [1].

Due to their ability to deliver high flow rates, electronic insufflators are preferred for complex surgical procedures. However, in diagnostic surgical cases where flow rates of less than 4 L/min are required, pneumatic insufflators are more practical. Many types of actuators and control systems are required to control and operate insufflators in today's rapidly developing technology. In medical insufflators, there are two sources of power that are important for the operation of the instrument - electrical and pneumatic [1].

II.4 pressure control in medical devices

To control the pressure in medical devices we should know the laparoscopic insufflators function to control the flow of CO_2 gas into the abdominal cavity to create and maintain the capnoperitoneum. Pressure Settings the required CO_2 pressure is between 10 and 15 mmHg the pressure must be carefully regulated to provide enough space for surgical instruments and visualization without causing undue stress on the patient's body [20]. The Continuous monitoring of the capnoperitoneal pressure is crucial, the capnoperitoneal pressure was continuously monitored at 0.1 Hz using a high-precision pressure probe connected to trocar. the stability of the capnoperitoneal pressure is influenced by the type of smoke management technology use [21]. Five surgical smoke management technologies:

"A: continuous passive venting; **B**: continuous passive filtration; **C**: continuous active; **D**: circular filtration; **E**: continuous electrostatic aerosol precipitation. " [21].

Figure II.2: Photographic images of the examined surgical smoke management technologies [21].

II.4.1 impact of smoke management technologies

-Active Filtration this method can lead to unstable capnoperitoneal pressure due to high CO_2 flow rates, which can interfere with surgical procedures.

-Electrostatic Precipitation this technology maintains a stable capnoperitoneum with minimal CO_2 consumption, making it highly effective for pressure control [22].

II.4.2 leakage control & safety and efficacy

Minimal access surgery uses trocar systems to insufflate the abdomen with CO_2, creating space for operation. Traditional (valved) trocars prevent gas leakage but can complicate instrument removal and lens contamination. New valveless systems maintain pressure using a pressure barrier and allow continuous gas flow [23]. Surgeons should verify haemostasis, ideally at lower intra-abdominal pressure and adequate blood pressure to avoid false reassurance. Internal defects and port sites (especially 15 mm and most 10–12 mm ones) should be closed, unless in specific cases like severe obesity. After port removal, all sites should be checked for bleeding. A final surgical count with the team, including instruments and retrieval bags, is essential. The surgeon should take a moment at the end to mentally review the procedure, ensuring no planned steps or foreign objects are missed [24].

II.5 PID Control Theory

II.5.1 A Concise Explanation

By far the most common form of feedback control is proportional-integral-derivative (PID) control. In spite of the extraordinary advances that have taken place in theory of control over the past 20 years, industrial engineers, consider much control theory esoteric and of little relevance to industrial problems. In the early 1980s, the state of the art in industrial PID control was the tuning formulas proposed by Ziegler and Nichols 40 years earlier with the exception of Foxboro´s EXACT controller, modern attempts to develop automatic PID tuning have been model-based. Based on heuristic logic developed from computer simulation studies this controller was Introduced in 1984; The classical method of Ziegler and Nichols is the basis of the relay tuning method proposed by Åström and Hägglund in 1984. in this relay tuning method, the PID parameters of the controller are calculated using the knowledge of only one point on the open loop Nyquist curve. by increasing the gain of a proportional controller until a sustained oscillation of constant amplitude is obtained, the point of intersection of the Nyquist curve with the negative real axis is determined. The fact that the user cannot control the amplitude of the resulting oscillation is a disadvantage of this method. the realization that this point could be determined by replacing the proportional controller with a relay was Åström and Hägglund's ingenious idea. The relay will cause a limit cycle to occur when the loop is closed. with the amplitude [25].

II.5.2 PID Algorithms

The main PID design algorithms come in three forms: standard, parallel, and classical. There are several variations or modifications of these algorithms. The way the controller gain is specified is the main difference between these three algorithms. Parallel form has proportional gain affecting only proportional part of the signal. While the other two forms have a controller gain that is applied to all three of the terms. The following are considered for better performance:

- The derivative part is most often applied to the output of the process.
- The proportional part will only act on a fraction of the reference part.
- Integral action kept within saturation action of control variables (anti-windup)
- Bumpless or smooth transition from manual to automatic (or when changing parameters) [26].

II.5.2.1 Standard or Non-interactive form of PID Controller

The standard form is also called the standard or ISA algorithm. Some texts refer to it as the extended form, and it's the form used in MATLAB. According to formula (II.1), and the equivalent form of the transfer function in equation (II.2), the controller parameters of interest are Proportional Gain, K_p, Integral Time, Ti, and Derivative Time, Td. The expression "e" is the control error, which is the difference between the setpoint and the process output. That is, it's a summation of proportional, integral, and derivative parts. (Figure II.3) shows the internal structure of the algorithm. As shown in equations (II.1) and (II.2), the standard PID can be represented in the time and frequency domain respectively [26].

$$u(t) = Kp\left[e + \frac{1}{Ti}\int edt + T_d\frac{de}{dt}\right] \quad \text{(II.1)}$$

$$hc(s) = \frac{u(s)}{e(s)} = Kp\left[1 + \frac{1}{T_i s} + T_d s\right] \quad \text{(II.2)}$$

This text describes a controller where K_p is the proportional constant, Ti is the integral time, and Td is the derivative time. The controller's input and output are e(t) and u(t) in the time domain, and e(s) and u(s) in the frequency domain. The controller's behavior is represented by its Laplace transfer function, denoted as h(s) equation (II.2) [26].

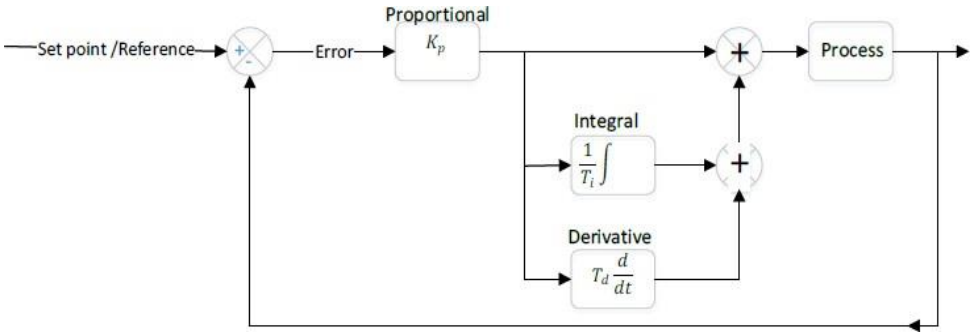

Figure II.3: The ideal or ISA PID algorithm [26].

It's also called the non-interactive, expanded. In this form the proportional gain affects all the three parts.

II.5.2.2 Parallel / Ideal form of PID Controller

The parallel algorithm is easy to understand. However, it is difficult to tune using traditional tuning methods such as Z-N and Cohen-Coon. Unlike other algorithms that have a gain that affects three terms, the controller has a gain factor that affects only the proportional part. But it can be transformed into an equivalent standard form where the parameter values are given by Eq. (II.3) and (II.4).

$$u(t) = K_p^p \times e + T_i^p \int e.dt + T_d^p \frac{de}{dt} \quad \text{(II.3)}$$

$$hc(s) = K_p^p + \frac{T_i^p}{s} + ST_d^p \quad \text{(II.4)}$$

"Where K_p^p is the proportional constant,T_i^p i is the integral time and T_d^p is the derivative time for the parallel form. The superscript 'p' is used to indicate the parallel form of the PID." [26]

$$K_p^p = K_p \; ; T_i^p = \frac{k_p}{T_i} ; T_d^p = K_p T_d \quad \text{(II.5)}$$

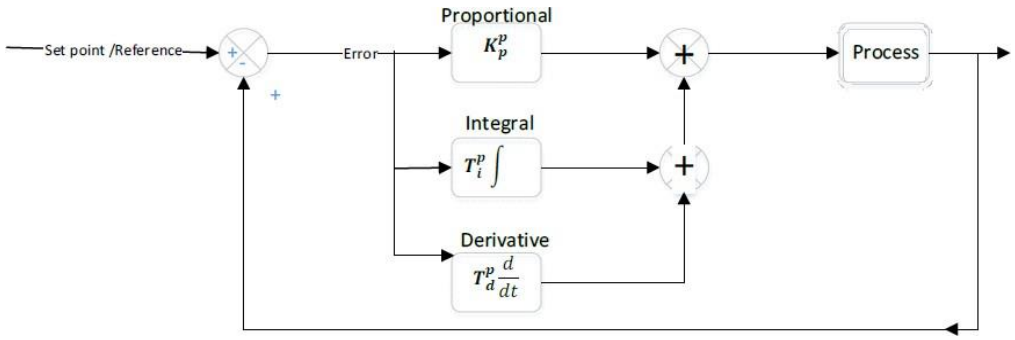

Figure II.4:The Parallel form of PID algorithm [26].

The gain affects only the proportional part as compared to the standard form where the proportional gain is affect both the integral and derivative parts

II.5.2.3 Series/Classical / Interacting form of PID Controller

In this form, the PI and PD elements are operated in series, also known as a series, cascade, real or interactive PID controller. The parameters of the controller interact with each other. The integral time influences the derivative terms and verse visa. Equations (II.6) and (II.7) are the differential and transfer function equations of the controller, respectively. The internal structure of the controllers is shown in (Figure II.5). The interacting and non-interacting forms are the same for P, PI or PD only regulators, the two forms are equivalent if the derivative time is much smaller than the integral part. the choice of forms to be used depends on the manufacturer and the operator needs to understand this for better tuning to ensure optimal performance [26].

$$u(t) = K_c \left[e + \frac{1}{T_i^s} \int e.dt\right] \times \left[1 + T_d^s \frac{de}{dt}\right] \quad \text{(II.6)}$$

$$hc(s) = Kc \left[1 + \frac{1}{T_i^s s}\right] \times \left[1 + T_d^s s\right] \quad \text{(II.7)}$$

"Where K_c is the proportional constant, T_i^s is the integral time and T_d^s is the derivative time. The superscript 's' is used to indicate the series form of the PID."[26]

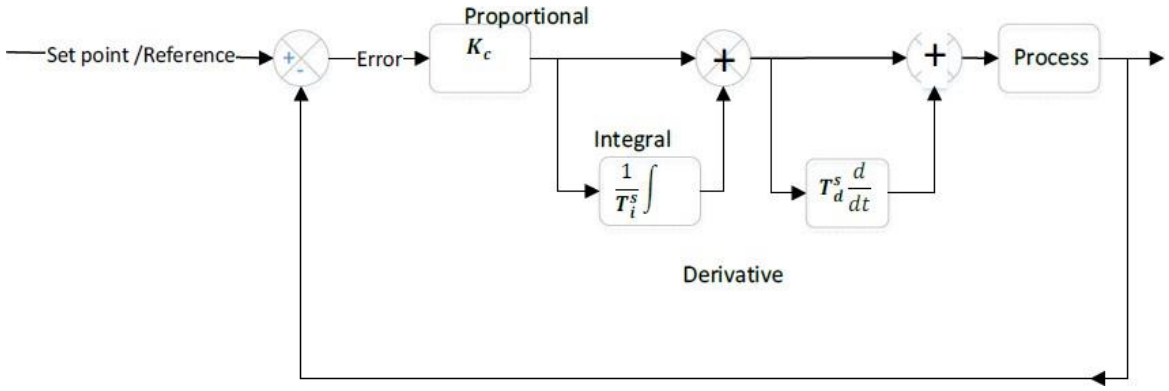

Figure II.5: Series or interacting PID form [26].

It's also called the cascade real form. The PID parts interact with each other; the integral part interacts with the derivative part and vice versa

II.6 PID Controller Structure & Basics

II.6.1 Controller structure

In the following, it is assumed that the controller has the parallel structure. This is defined as:

$$Hc(s) = K_p(1 + \frac{1}{\tau_I} + \tau_D s) \quad \text{(II.8)}$$

Assume the control setup of (Figure II.6), where y is the process output, n is the measurement noise, r is the reference or setpoint, e is the tracking error, d is the load disturbance, and u is the plant input [27].

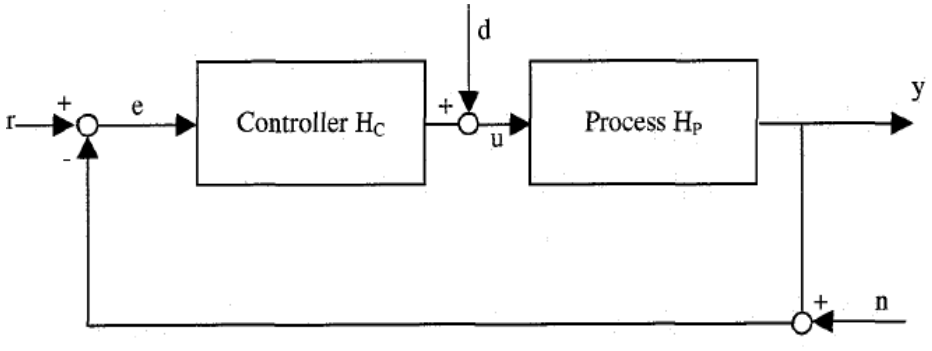

Figure II.6: Control configuration [27].

II.6.2 Feature based methods

Many tuning methods based on a few features of the process dynamics that can be easily obtained experimentally are presented in the literature. Step response parameters are typical time domain features [27].

- **Ziegler-Nichols step response method (1942)**

The first Ziegler-Nichols tuning method, known as the process reaction curve method, is a simple way to tune PID controllers based on the step response of a system. By applying a step input and analyzing the resulting output curve, two key parameters are measured: the delay time (θ) and the slope of the steepest tangent (a). These values are then used in predefined formulas to calculate the PID gains. The goal is to achieve a quarter decay ratio, which offers a good balance between fast response and system stability. Despite its simplicity, this method remains popular for its practical effectiveness [27].

- **Ziegler-Nichols continuous cycling method**

The Ziegler-Nichols frequency-domain method uses the ultimate gain (Ku) and ultimate period (Tu) to set PID parameters. It involves pushing the system to the edge of instability, which can be risky. This method may also produce varying results depending on the process characteristics [27].

- **Cohen-Coon method (1953)**

The Cohen-Coon method uses three open-loop step response parameters (θ, τ, and K) to tune PID controllers, focusing on rejecting load disturbances. It aims for a quarter decay ratio by positioning closed-loop poles accordingly. Although it includes more information than Ziegler-Nichols, its performance is similar, often resulting in under damped systems due to a low decay ratio [27].

- **Århröm and Hägglund (1985)**

Århröm and Hägglund observed that the Ziegler-Nichols continuous cycling method identifies the point (−1/Ku, 0) on the Nyquist curve and shifts it to a predefined location. With PID control, this point can be moved to any desired position: increasing the gain shifts it toward

G(jω) while adjusting the integral or derivative actions moves it in a perpendicular direction [27].

II.7 Optimization based methods

II.7.1 Minimum optimization criterion

There are many methods presented in the literature that are designed to minimize a certain error criterion. The minimum ITAE method is discussed here to illustrate these methods. ITAE is acronym for Integral of the Time Weighted absolute Error, and is defined as follows:

$$\text{ITAE} = \int_0^\infty t|e(t)|dt \tag{II.9}$$

Since the initial error for a step response is always large, time weighting is used. And for most cases of setpoint tracking it is reasonable to have less weight on this error, "a distinction is made between responding to a disturbance or responding to a set point", (Table II.1) shows the controller settings that provide a minimum ITAE [27].

Table II.1:Controller settings for minimum ITAE [27].

Type of input	Controller type	K_p	τ_I	τ_D
Disturbance	P	$\frac{0.49}{K}[\frac{\tau 1}{\theta}]^{1084}$	-	-
	PI	$\frac{0.859}{K}[\frac{\tau 1}{\theta}]^{0.977}$	$\frac{\tau 1}{0.674}[\frac{\tau 1}{\theta}]^{-0.680}$	-
	PID	$\frac{1.357}{K}[\frac{\tau 1}{\theta}]^{0.947}$	$\frac{\tau 1}{0.842}[\frac{\tau 1}{\theta}]^{-0.738}$	$0.381\tau 1\,[\frac{\tau 1}{\theta}]^{-0.995}$
Setpoint	PI	$\frac{0.586}{K}[\frac{\tau 1}{\theta}]^{0.916}$	$\frac{\tau 1^2}{1.03\tau 1 - 0.165\theta}$	-
	PID	$\frac{0.965}{K}[\frac{\tau 1}{\theta}]^{0.855}$	$\frac{\tau 1^2}{0.796\tau 1 - 0.147\theta}$	$0.308\tau 1\,[\frac{\tau 1}{\theta}]^{-0.929}$

II.7.2 LQR optimization of ISE

To minimize the ISE criterion, which is the integral of the squared error, Argelaguet used LQR optimization. The FOLPD model with a first-order Padé approximation for the time delay is used in this optimization. the tuning rules that result from the minimization are the same as the IMC tuning rules for this model [27].

II.7.3 Constrained optimization

Panagopoulos maximizes the integrated error (IE) by minimizing the ratio $\frac{K_p}{\tau_I}$ assuming these variables are directly related for a step load disturbance. This optimization is performed without imposing strict constraints on the maximum sensitivity M_s, allowing for more flexibility in tuning. Instead of using a fixed grid, an adaptive method is used to explore combinations of K_p, $\frac{K_p}{\tau_I}$, and $K_p \times \tau_D$, even if they slightly exceed traditional robustness limits. This approach prioritizes fast setpoint tracking over robustness. The setpoint response is fine-tuned manually, without relying on setpoint weighting. In contrast, Ingimundarson employs a completely different method, relying heavily on frequency-domain criteria and removing the Nyquist smoothness constraint to allow more aggressive controller behavior [27].

II.8 Model-Based design

II.8.1 Internal Model Control, IMC

The IMC method explicitly uses the process model in the design of the controller. it is a general design approach, applicable to various systems. for low-order process models, the IMC method typically results in PID controllers. the controller is formulated as:

$$Hc(s) = \frac{Hf(s)H^{-1}p_{-}(s)}{1-Hf(s)H^{-1}p_{-}(s)Hp(s)} \quad \text{(II.10)}$$

Where $M_p = H_p \text{h} H_p$, and $Hp_{+}(s)$ includes all non-minimum phase dynamics .$Hf(s)$is a low-pass filter" typically selects as:

$$Hf(s) = \frac{1}{\lambda s+1} \quad \text{(II.11)}$$

Such a controller cancels the process poles and zeros, and tends to be highly ordered. However, the procedure results in a PI or PID controller when the order of the model is low. for example, using the FOLPD model with a first-order Padé time delay approximation, the controller becomes [27].

$$\mathrm{Hc} = \frac{1}{\mathrm{K}} \frac{(\tau 1 s+1)(0.5\theta s+1)}{(\lambda+0.5\theta)s} \tag{II.12}$$

which, after a few manipulations, results in the following for the PID parameters

$$Kp = \frac{1}{k} \frac{(\tau 1+0.5\theta)}{(\lambda+0.5\theta)}; \quad \tau 1=\tau 1+0.5\theta; \quad \tau \mathrm{d} = \frac{\tau 1 \theta}{2\tau 1+\theta} \tag{II.13}$$

With this controller, the closed loop is:

$$H_{cL}(s) = \frac{1}{\lambda s+1} \tag{II.14}$$

A single parameter, ζ, provides a clear tradeoff between robustness and performance when designing PID controllers with IMC. As opposed to traditional PID which has three parameters that are difficult to interpret, IMC provides good tracking of the setpoint but it can result to sluggish disturbance rejection when the slow poles are canceled. There are several IMC-based PID design methods available in the literature, including adaptations for unstable systems and for integrating systems.

And the handling of time delays by means of Maclaurin approximations. Skogestad, who proposed simple IMC-based tuning rules, introduced a notable simplification [27].

II.9 PID Auto-Tuning Methods

PID auto-tuning simplifies the task of manually adjusting PID loops in process plants, saving time and reducing production downtime. Three main approaches to PID auto-tuning are discussed: gain scheduling, model-based adaptive tuning, and the relay feedback experiment. The goal of auto-tuning is to create a point on the Nyquist curve to help identify changing system parameters. Relay auto-tuning works by causing the system to oscillate, either by replacing the controller with a relay or integrating a relay into the feedback loop. Variations like adding hysteresis to the relay can improve parameter estimation. The amplitude and frequency of the resulting sustained oscillations are used to tune the controller. This method is simple to apply in closed-loop systems and can be initiated with just a push button.

The autotuning procedure consists of three main steps as reported, these are:

- The generation of process disturbance/oscillation intentionally by the operator.
- Automatic evaluation or computation of the disturbance dynamics.
- The usage of the disturbance response to re-evaluate the controller parameters.

In the relay feedback experiment, the oscillation amplitude is controlled by the relay's amplitude to generate a limit cycle at the process's critical point. This helps avoid uncontrolled oscillations that could damage equipment.

Although modifications allow identification at other points, noise and hysteresis can affect accuracy, requiring further adjustments and calculations. To analyze the relay excitation of the process, there are two main methods:

- Limit Cycle analysis.
- Describing functions [26].

II.9.1 Relay

Relays have been used as amplifiers since the fifties, but were not applied to adaptive control until the sixties. Relay autotuning has the following advantages:

- It’s easy to automate by switching from the controller to the relay during auto tuning operation.
- No loop instability introduced by the method.
- Minimal prior knowledge of the process required.
- Process error during tuning can be minimized by selecting the correct relay parameters [26].

II.9.2 Ultimate Period and Gain from Relay Experimentation

II.9.2.1 Limit cycle Oscillation

Limiting Cycle is a path for which the energy remains constant without being lost or gained in a system. The process quickly reaches the limit cycle oscillation due to the nonlinearity of the relay. The linear systems under memory effects can also cause limit cycle oscillations. The principle of limit cycling is a key input to the analysis of the descriptive

function, The nonlinearity in a relay as shown in equation (II.15) will produce a persistent excitation. which causes the linear element output to oscillate as follows:

Given a state space of the process, such as the one given by (II.15), a limit cycle is generated when the condition in equation (II.19) is true.

$$\dot{x} = Ax + Bu; y = Cx \tag{II.15}$$

If the process exhibits a limit cycle with period T, the relay switches states at intervals of Δt=T/2, meaning it changes state every half-cycle as shows in equation (II.16).

$$\frac{x_{k+1}-x_k}{\Delta t} = Ax_{k+} Bu_k ; \Delta t = t_{k+1} - t_k = \frac{T}{2} \tag{II.16}$$

The relay output d serves as the process input. By resolving equation (II.16), equation (II.17) is obtained. Due to the symmetric nature of the limit cycle, the inputs at times k and k+1 are related as shown in equation (II.18).

$$x_{k+1} = \Phi x_k + \gamma d$$

$$\text{Where } \Phi = (I + \frac{T}{2}A) \text{and} \gamma = \frac{\text{BT}}{2} \tag{II.17}$$

$$x_{k+1} = -x_k \tag{II.18}$$

Substituting equation (II.18) into equation (II.17) and solving for the output in equation (II.15) leads to equation (II.19), which represents the condition required for a limit cycle to occur [26].

$$\text{C}(\text{I} + \Phi)^{-1}\gamma = 0 \tag{II.19}$$

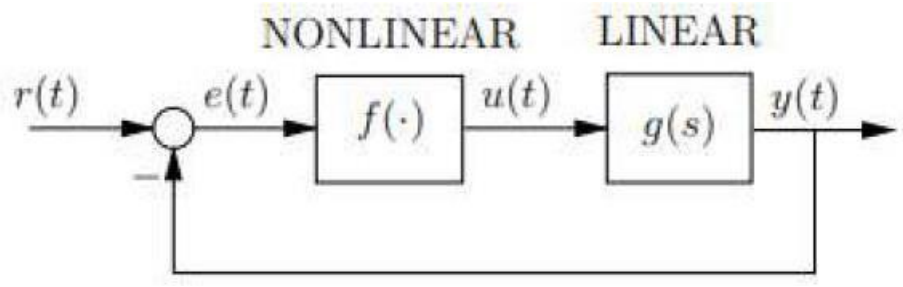

Figure II.7: A nonlinear element f (.) such as a relay will drive the linear element g(s) into oscillation [26].

II.9.2.2 Describing function analysis (DF)

The describing function is used to analyze limit cycle behavior in nonlinear systems, providing a reliable estimate. It is defined as the ratio of the fundamental component of the relay output to the sinusoidal input, which is described by equation (II.20).

$$e(\theta) = a\sin\theta\,;\ \theta = \omega t \tag{II.20}$$

The Fourier series expansion of the periodic output signal is given by equation (II.21):

$$f(\theta) = a_0 + \sum_{n=1}^{\infty}(a_n \cos n\theta + b_n \sin n\theta) \tag{II.21}$$

Where the fundamental component is given by equation (II.22):

$$a_0 = \int_0^{\pi} e(\theta)d\theta \tag{II.22}$$

The harmonics components are given in equation (II.23) and (II.24):

$$a_n = \int_0^{2\pi} e(\theta)\cos(n\theta)\,d\theta \tag{II.23}$$

$$b_n = \int_0^{2\pi} e(\theta)\sin(n\theta)\,d\theta \tag{II.24}$$

Assuming the nonlinearity's output is sinusoidal and symmetric about the origin, the coefficients a_0 and a_n become zero, simplifying equation (II.21).

$$f(\theta) = \sum_{n=1}^{\infty} b_n \sin(n\theta)\,d\theta \tag{II.25}$$

$$b_n = \frac{2}{\pi}\int_0^{\pi} d\,\sin(n\theta)d\theta \tag{II.26}$$

Solving equation (II.26) gives equation (II.27) for odd harmonics and zeroes for even harmonics:

$$b_n = \frac{4d}{n\pi} \tag{II.27}$$

Thus equation (II.28) becomes which is the output of the relay:

$$f^r(\theta) = \sum_{n=1}^{\infty} \frac{4d}{n\pi}\sin(n\theta) \tag{II.28}$$

And the ratio of equation (II.28) to (II.20) at the fundamental component gives the describing function N(a).

$$N(a) = \frac{outputofrelay}{inputofrelay} = \frac{f^r(\theta)}{e(\theta)} = \frac{4d}{a\pi} \quad \text{(II.29)}$$

The system exhibits continuous cycling or marginal stability when the open-loop transfer function equals zero, meaning the closed-loop input and output have the same amplitude and phase. This condition is represented by equation (II.32).

$$1 + N(a)G(iw_u) = 0\ ; G(iw_u) = -\frac{a\pi}{4d} \quad \text{(II.30)}$$

The ultimate gain, Ku and ultimate period, and ultimate frequency are given in Eq:

$$k_u = \frac{4d}{n\pi}\ ;\ P_u = T_u\ ;\ w_u = \frac{2\pi}{T_u} \quad \text{(II.31)}$$

where Tu is the period of the sustained oscillation at the approximate cross-over frequency [26].

II.9.2.3 Åstrom Relay Method

Åstrom's relay feedback method offers an alternative to the Ziegler-Nichols tuning approach by inducing controlled oscillations using a small relay signal, typically 2% to 10% of the control effort. This avoids the risk of pushing the system into instability. The relay output, which serves as the control input, switches between positive and negative values. However, this method is unsuitable for systems that cannot handle negative inputs, such as air heaters. System gain and frequency are determined through a specific equation [26].

II.9.2.4 Schei Relay method

The Schei method, similar to Åstrom's, uses relay feedback for PID tuning, assuming a stable controller is already in place. The reference signal switches between positive and negative relay values, causing the control signal to vary and generate a limit cycle. A filter is included in the derivative loop to reduce the impact of noise. The method's implementation is illustrated in a block diagram and validated through simulation results [26].

II.10 Conclusion

The chapter highlights the essential interplay between biomedical engineering and control systems. Effective pressure regulation mechanisms are therefore critical components of modern medical devices. The implementation of PID control theory offers a robust solution for maintaining stability and precision in such systems by continuously monitoring and adjusting system outputs in response to real-time feedback, PID controllers contribute significantly to the reliability, safety, and performance of medical technologies.

Chapter III

PID Pressure Control Modeling in MATLAB/Simulink

III.1 Introduction

In this chapter we will see how the CO2 insufflation system works using MATLAB/Simulink Simscape. While Simulink is a graphical programming environment inside MATLAB, used for modeling, simulating, and analyzing dynamic systems and Simscape is a physical modeling toolbox within Simulink. The system uses controlled specific positive pressure optimizing for patient safety and surgical requirements, not ambient atmospheric pressure the PID controller dynamically maintains this specific pressure during insufflation [1].

III.2 Modeling and Simulation in MATLAB/Simulink

III.2.1 System design

The core motivation behind this project is to accelerate the development process of insufflators; the focus is on maintaining precise, stable pressures above atmospheric levels for safe and effective insufflation. Enhance their quality, and ensure compliance with FDA and German regulatory standards within a limited timeframe. Leveraging Model-Based Design through MATLAB/Simulink allows for efficient modeling and simulation of control strategies, enables code generation for real-time prototyping platforms, and supports the creation of optimized code suitable for deployment on embedded systems [1].

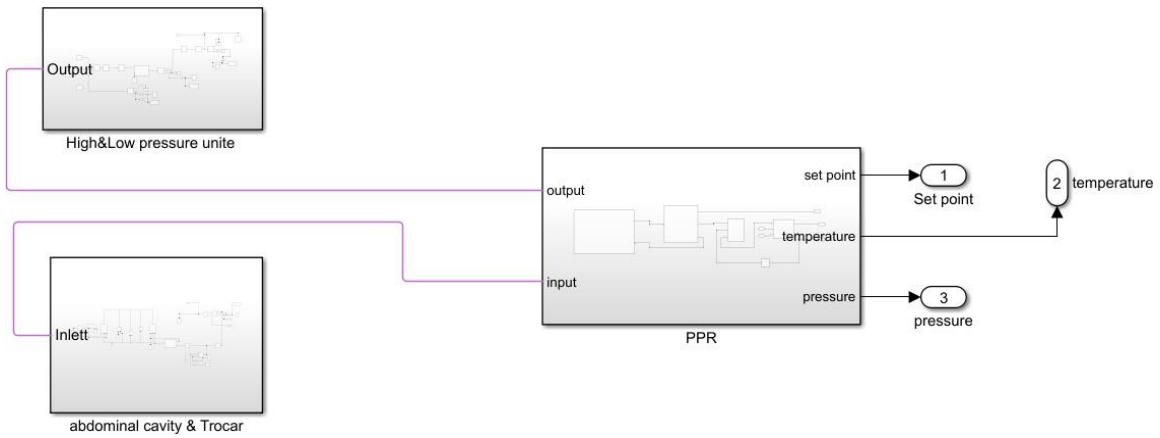

Figure III.1: CO2 insufflator MATLAB/Simulink model.

The system consists of 5 blocks: The high-pressure unit (HPU), the low-pressure Unit (LPU), the proportional pressure regulator (PPR), the trocar subsystem and the abdominal cavity model.

III.2.2 High-pressure unit (HPU):

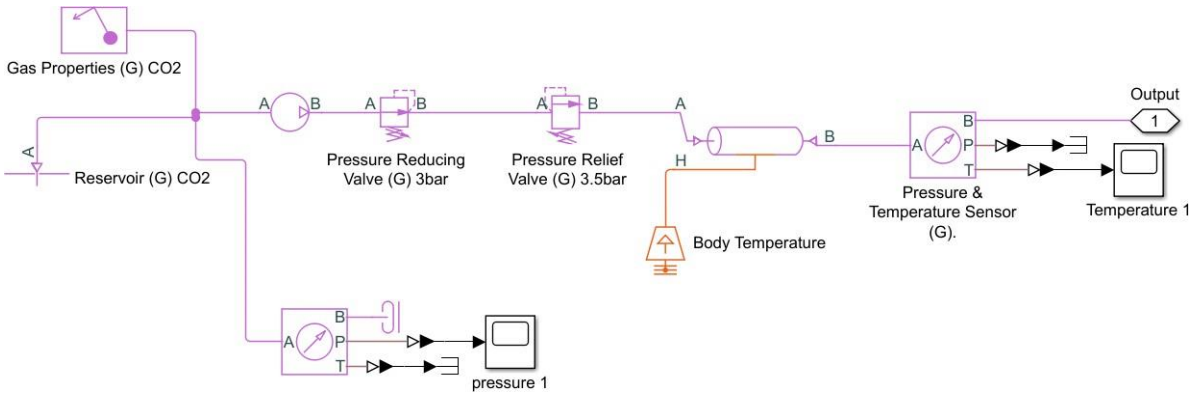

Figure III.2: HPU Simscape block diagram.

The initial stage of the system involves a medical CO_2 gas cylinder that stores carbon dioxide under high pressure approximately 50 bar and at a low temperature, close to -2 °C (273.15 K) inside the reservoir (G) and gas properties (G) defines the characteristics of the gas within the system. Instead of using a real-gas model [1]. The Mass Flow Rate Source (G) functions as a controlled mass flow rate generator. The mass flow rate is imposed, meaning that Simscape computes the pressure at the ports to ensure consistency with the rest of the system.

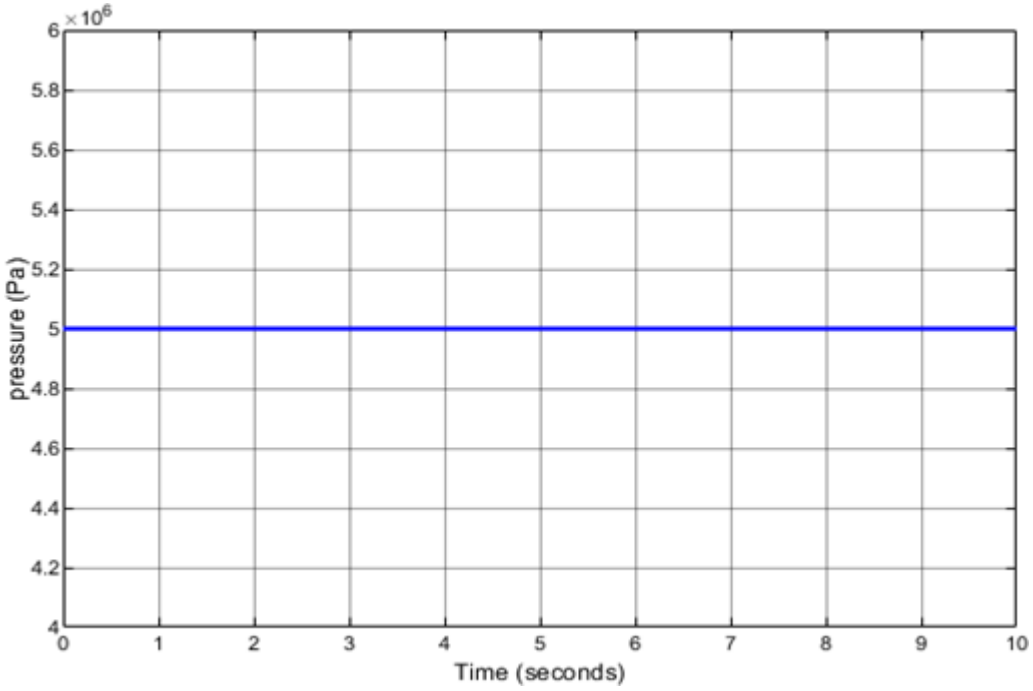

Figure III.3: P1 sensors reading.

We did make sure that the initial pressure is 50bar (5000 kPa); and we have the pressure reducing valve that will reduce the pressure from 50bar (5000 kPa) to 3bar (300 kPa) after the pressure reducing valve, a safety pressure relief valve of 3.5 bar (350 kPa) is used for safety, to prepare the CO_2 for medical insufflation, it must be warmed to body temperature around 37 °C to reduce patient discomfort during surgical procedures. This is achieved through a constant-temperature heat source, acting as a gas heater. a temperature sensor, T1, is installed to verify the effectiveness of the heating process, ensuring the gas reaches the desired thermal condition before entering the patient's abdominal cavity.

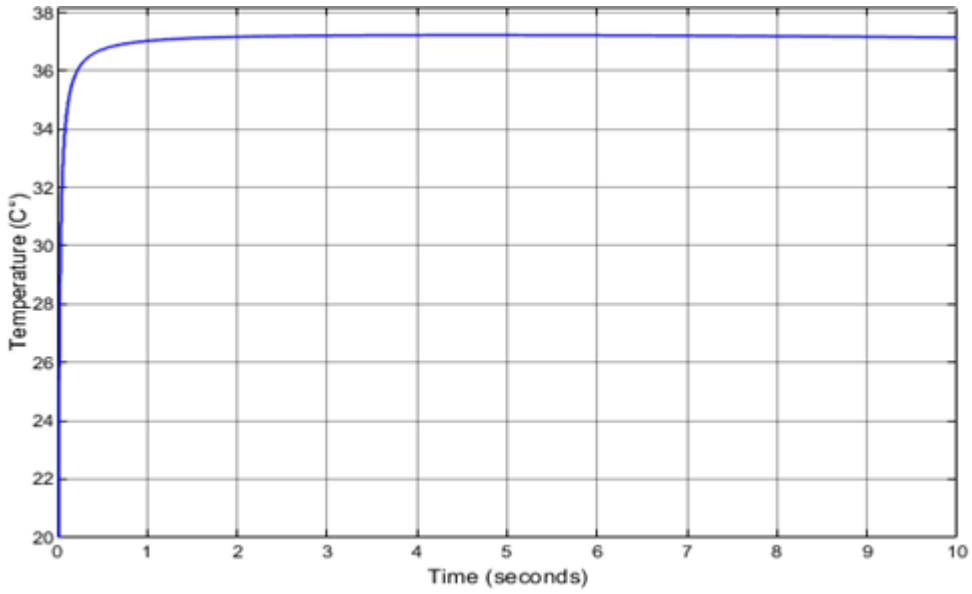

Figure III.4: T1 Sensor reding.

III.2.3 Low pressure unit (LPU)

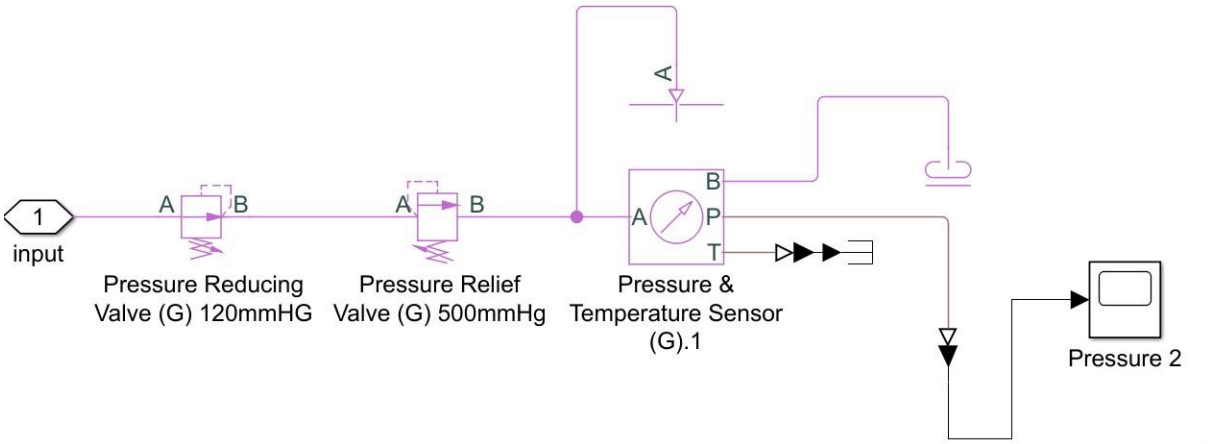

Figure III.5: LPU Simscape block diagram.

This block is made up of a pressure reducing valve and safety valve. The pressure reducing valve decreases the pressure from 3bar to around 0.16 bar (120 mmHg). The safety valve's operating pressure is around 0.66 bar (500 mmHg) .

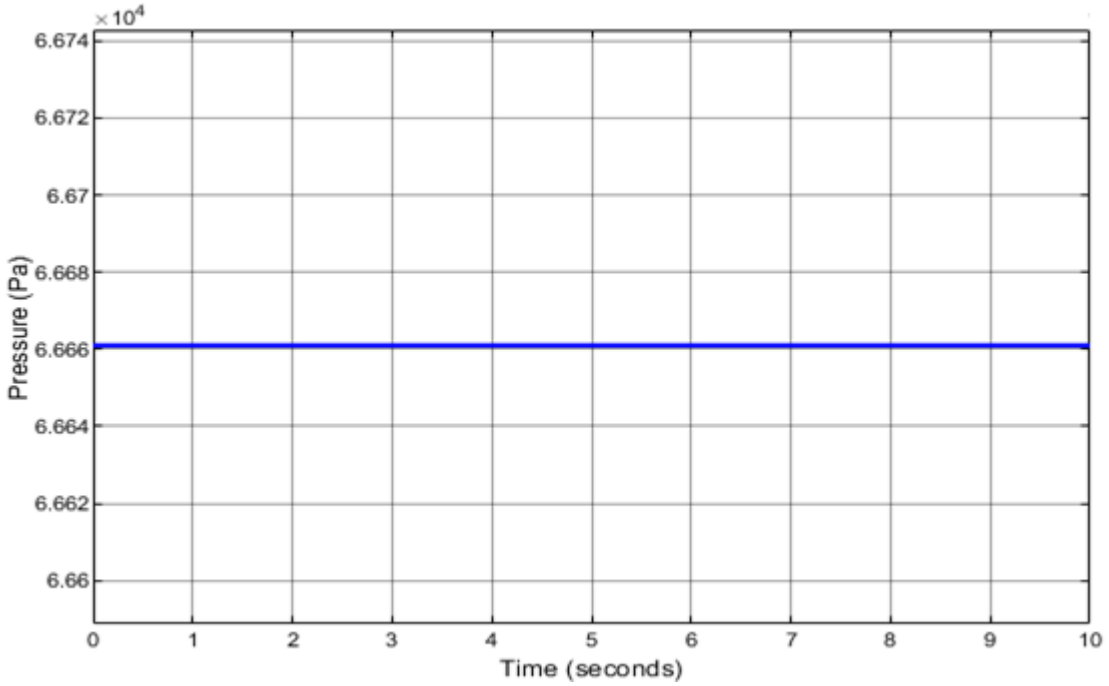

Figure III.6: P2 sensor reading.

We made sure that both the pressure-reducing valve (G) and the pressure relief valve (G) are working correctly. the (figure III.6) gave a 66660 Pa equal to 499.992 mmHg.

III.2.4 Abdominal cavity

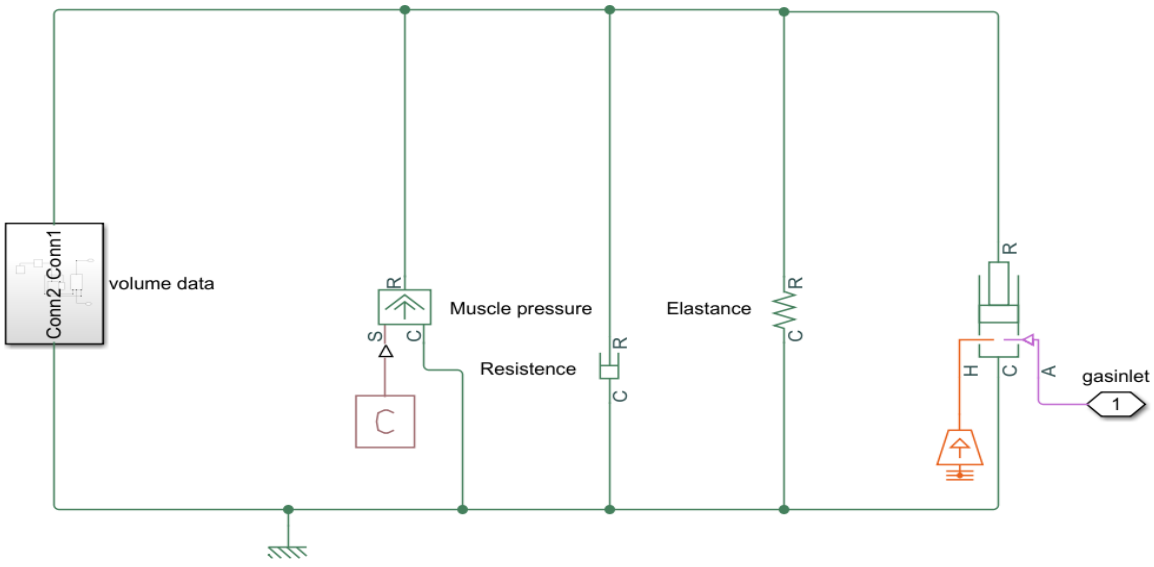

Figure III.7: Abdominal cavity Simscape sub-block diagram.

(Figure III.7) illustrates the Simscape sub-block diagram of the abdominal cavity.

In this setup, the Translational Mechanical Converter (G) functions to transform the pressure of CO_2 gas into a linear mechanical motion. By configuring the interface cross-sectional area, A to a unit value, the displacement observed in the translational mechanical network corresponds directly to the volume of CO_2 gas introduced into the cavity. In this context, the mechanical force generated is interpreted as the pressure exerted by the gas within the abdominal space.

Additionally, the spring element in the model is used to simulate abdominal elastance, reflecting the stiffness of the abdominal wall. The damper, on the other hand, is used to represent the abdominal resistance, modeling how the abdominal cavity resists the inflow or expansion caused by the insufflated gas [1].

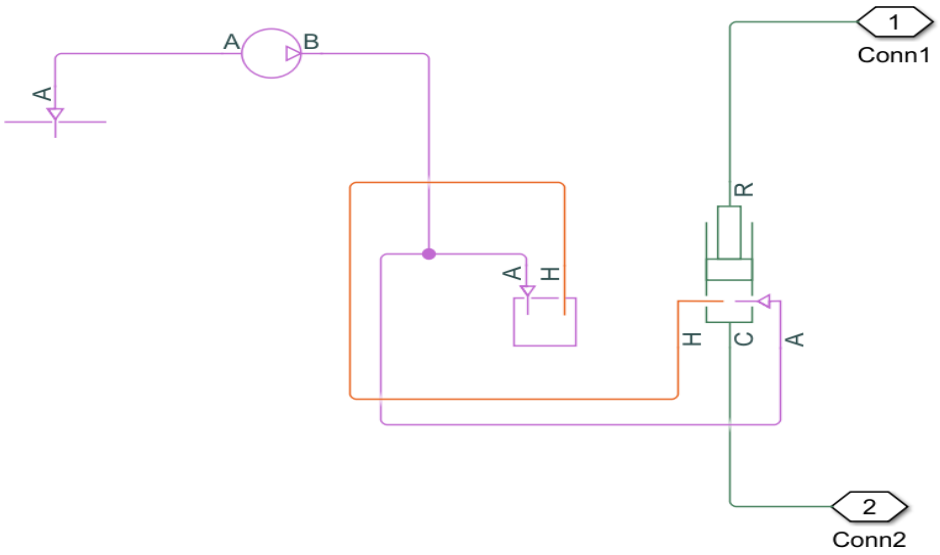

Figure III.8: volume data simscape.

The volume data in this (Figure III.8) represented the volume of CO2 gas delivered to the abdominal cavity via pressure-driven motion, and it being translated into mechanical displacement using a translation mechanical converter.

III.2.5 Trocar

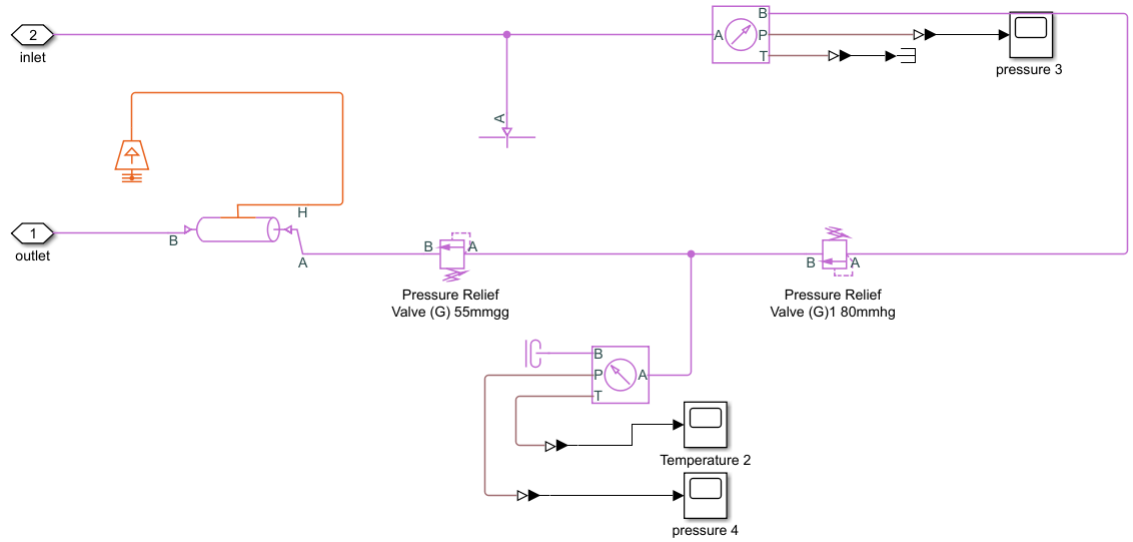

Figure III.9: Trocar Simscape sub-block diagram.

A trocar is a sharp tool that is usually placed inside a cannula, or tube, and used to pierce the body wall and provide access to the abdominal cavity or other internal spaces. The block consists of 2 sensors and tow pressure relief valve (G) in order to ensure the effectiveness of the system and the trocar is modeled as a pipe affected by the patient's body temperature.

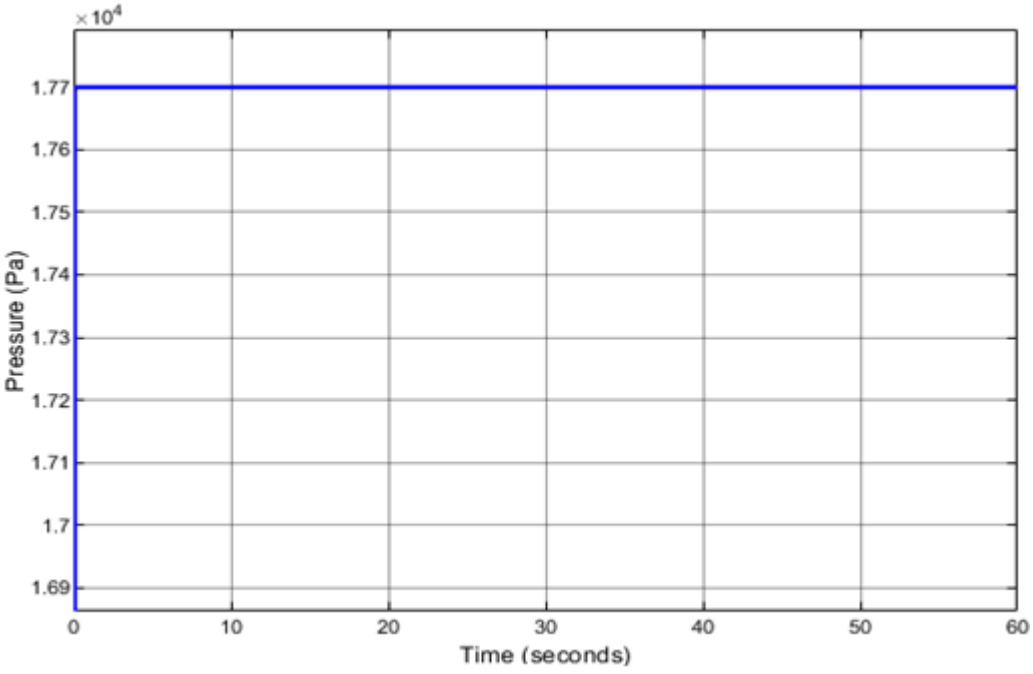

Figure III.10: P3 sensor reding.

In Figure III.10 :The pressure is greater than 80mmHg (10.665×10^3Pa) this is required.

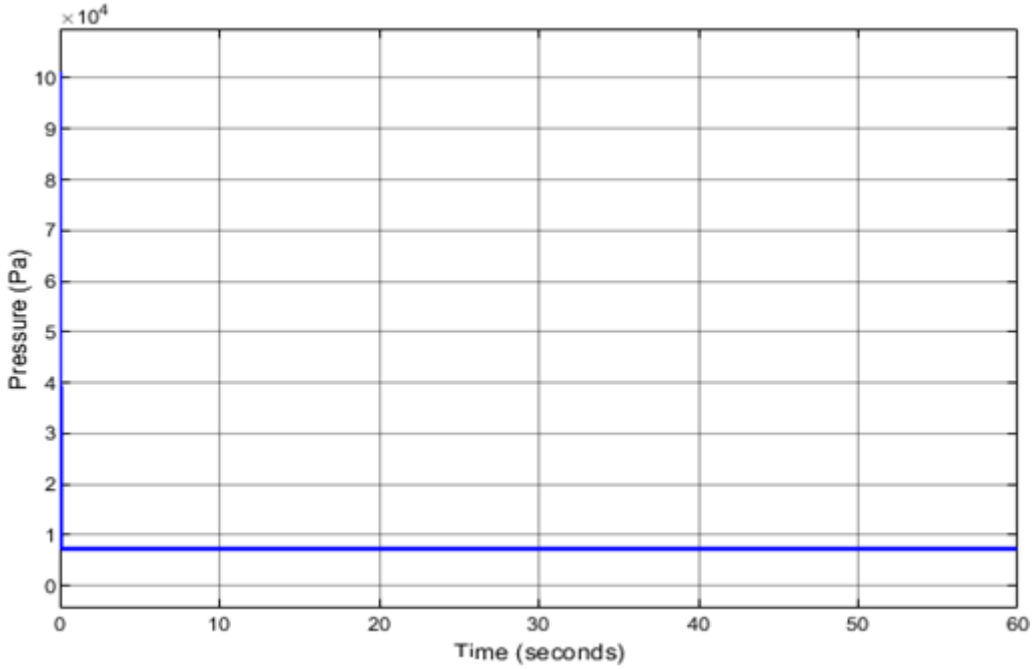

Figure III.11: P4 sensor reding.

In Figure (III.11) the pressure goes down to 7500 Pa equal to 56.25 mmHg, this confirms effectiveness of pressure relief valve (G).

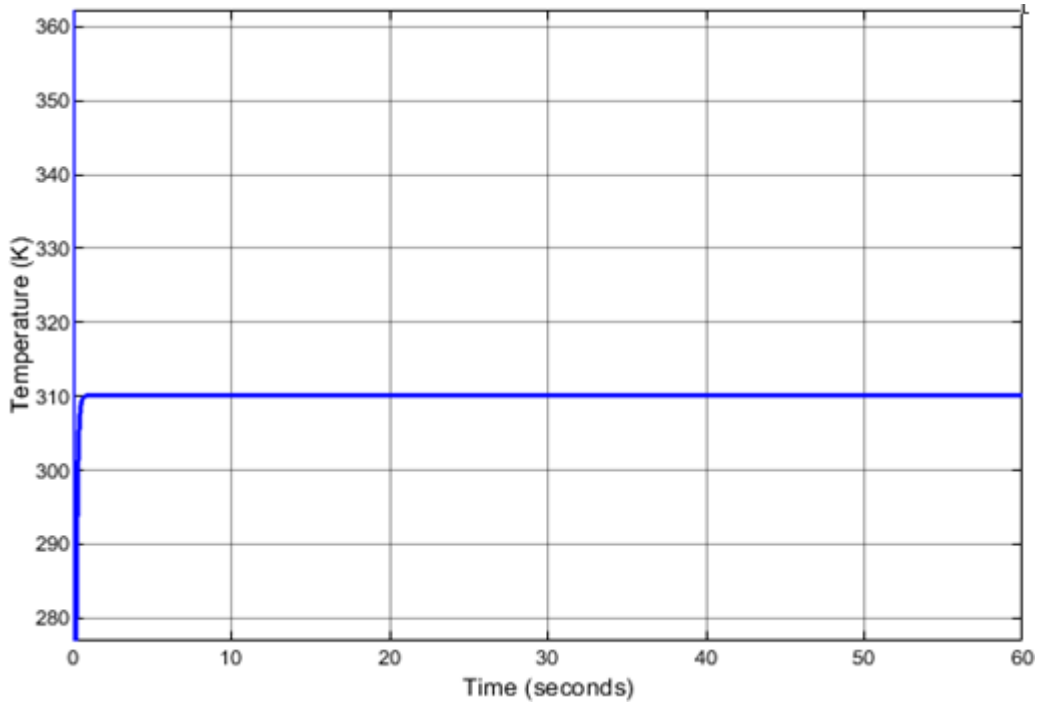

Figure III.12: T2 sensor reding.

The temperature from the (Figure III.12) is 310.15 K equal to 37C°, This ensures that we are introducing the appropriate temperature to the abdominal cavity, which is crucial for various medical procedures.

III.3 Implementing the Pressure PID Controller

III.3.1 Proportional pressure regulator (PPR)

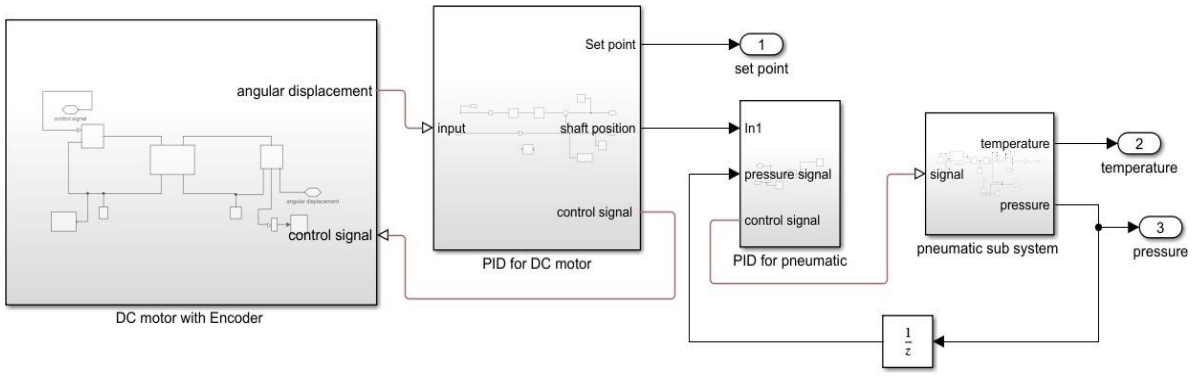

Figure III.13: PPR Simscape block diagram.

The block consists of: a DC motor with its encoder, Motor PID controller, and a PID controller for a mechanical pressure control valve. The DC motor is used to rotate the knob of a mechanical pressure control valve. And a unit delay to avoid an algebraic loop problem, The PPR block incorporates two PID (Proportional-Integral-Derivative) controllers to achieve the target output pressure. Manually tuning these controllers can be a complex and time-intensive task. By fully modeling the PPR system in MATLAB/Simulink, it becomes possible to analyze and optimize the system behavior in a virtual environment prior to physical production. This approach not only offers insights into the overall system performance but also aids in adjusting and refining the control parameters of each PID loop with greater efficiency [1,28].

III.3.1.1 PPR DC Motor with its PID controller Simscape Sub-block

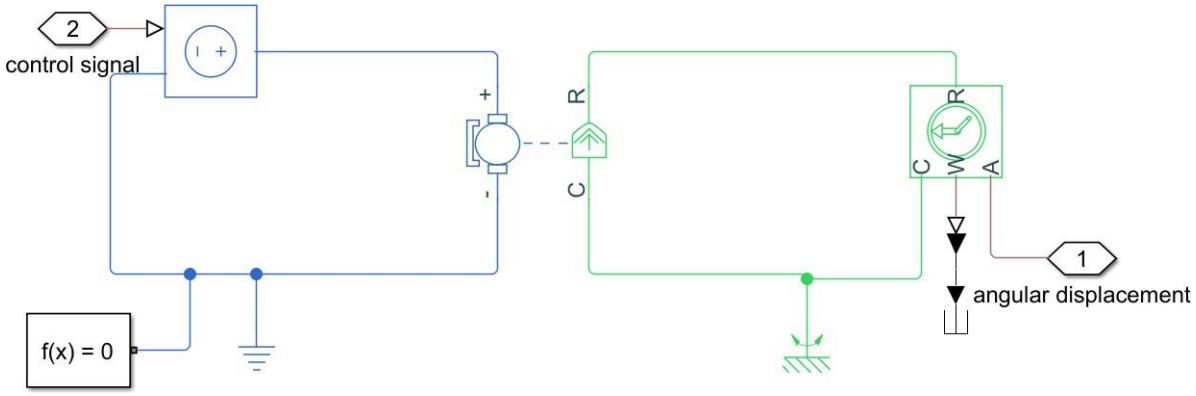

Figure III.14: PPR-DC motor Simscape sub-block diagram.

This subsystem includes a DC motor, a voltage source, and an ideal rotational sensor. The sensor monitors the motor's angular velocity. It provides feedback for use in a closed-loop control system. Rather than driving the motor directly, the PID controller's output is routed through a voltage regulator. This adjusts the motor's performance accordingly. The physical prototype uses an IG32 12V DC motor equipped with an encoder that operates at 100 rpm and delivers a tor que of 1.2 N.m.

III.3.1.2 PPR-DC motor PID controller Simscape sub-block

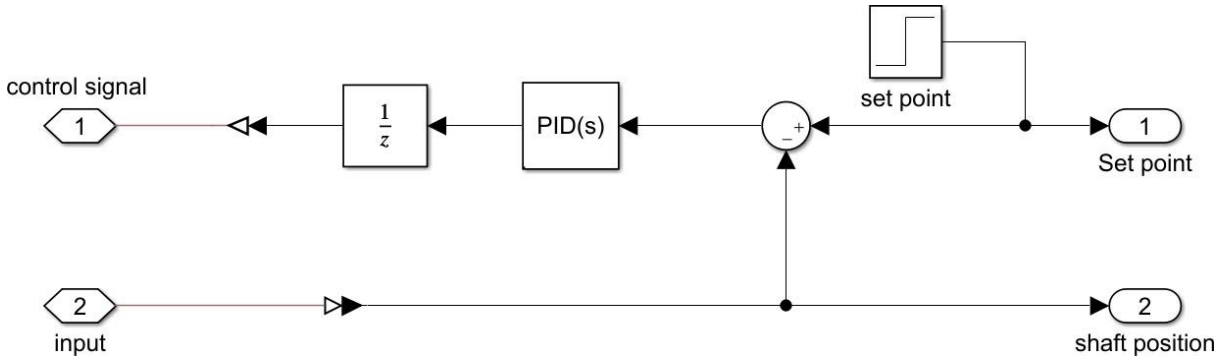

Figure III.15: PPR-DC motor PID controller Simscape sub-block diagram.

The pneumatic Simscape sub-block diagram features a PID controller used for closed-loop control of a DC motor. To enable signal processing in Simulink, a PS-to-S converter is included, which transforms the physical signal output from the ideal rotational sensor into a standard Simulink signal.

The reference (setpoint) signal is visualized using a scope for monitoring purposes. Additionally, a unit delay block is introduced into the loop to help prevent algebraic loop issues during simulation [1.28].

III.3.1.3 PID controller for the pressure regulator

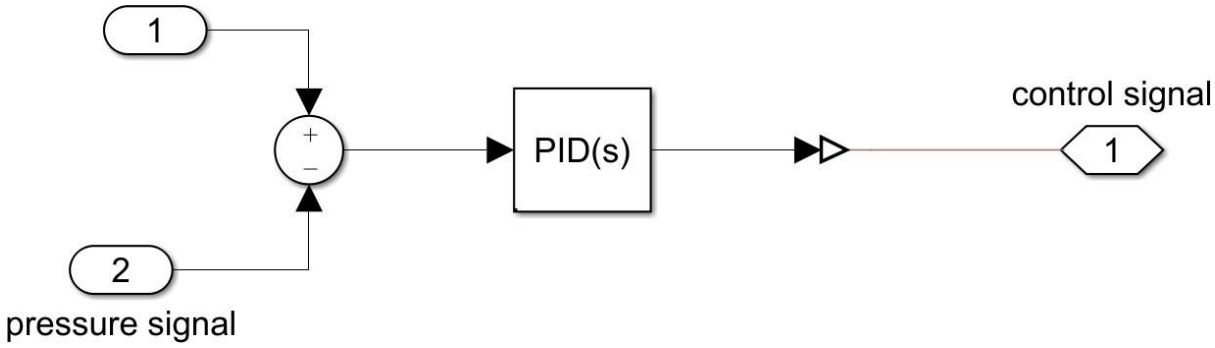

Figure III.16: Pressure regulator's PID controller Simscape sub-block diagram.

This sub-block includes a second PID controller dedicated to regulating the output of the pressure regulator. The input to this controller originates from the DC motor sub-block, where the pressure value is first converted into Pascals to serve as the setpoint. The resulting control signal from the PID controller is then passed through an S-to-PS converter, which transforms the Simulink signal into a physical signal suitable for the Simscape environment [1,28].

III.3.1.4 Pneumatic Simscape sub-block

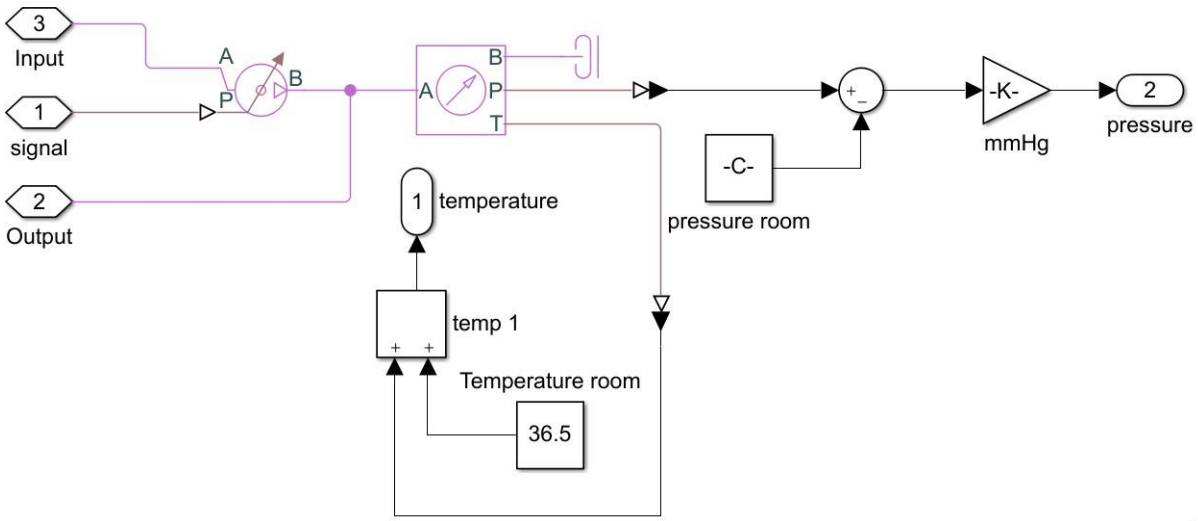

Figure III.17: Pneumatic Simscape sub-block diagram.

The controlled pressure block acts as a mechanical pressure regulator valve, operated through a PID controller. To enable closed-loop feedback control, pressure and temperature sensors are employed to monitor the output conditions of the CO_2 gas, specifically its pressure and temperature. These measurements are essential for ensuring accurate and stable regulation of the system. we chose the following values that gave an acceptable system response.

Table III.1: values used.

Pressure room	99499 Pa
Temperature room	36.5 K
Gain K	1/ 133.322
Kp	
Ki	1
Kd	1
N	100

III.3.2 PPR Results

- **Pressure**: in (Figure III.18) the pressure reading in the appropriate range which is 12-15 mmHg.

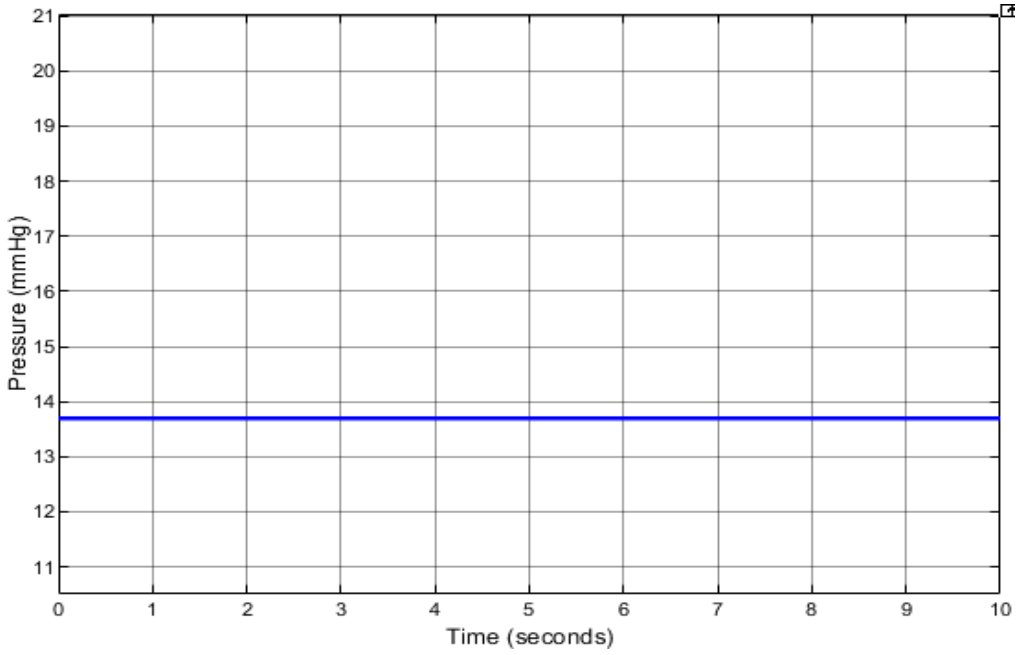

Figure III.18: PPR pressure reding value.

- **Temperature**: in the (Figure III.19) the Temperature value is required for patient safaty.

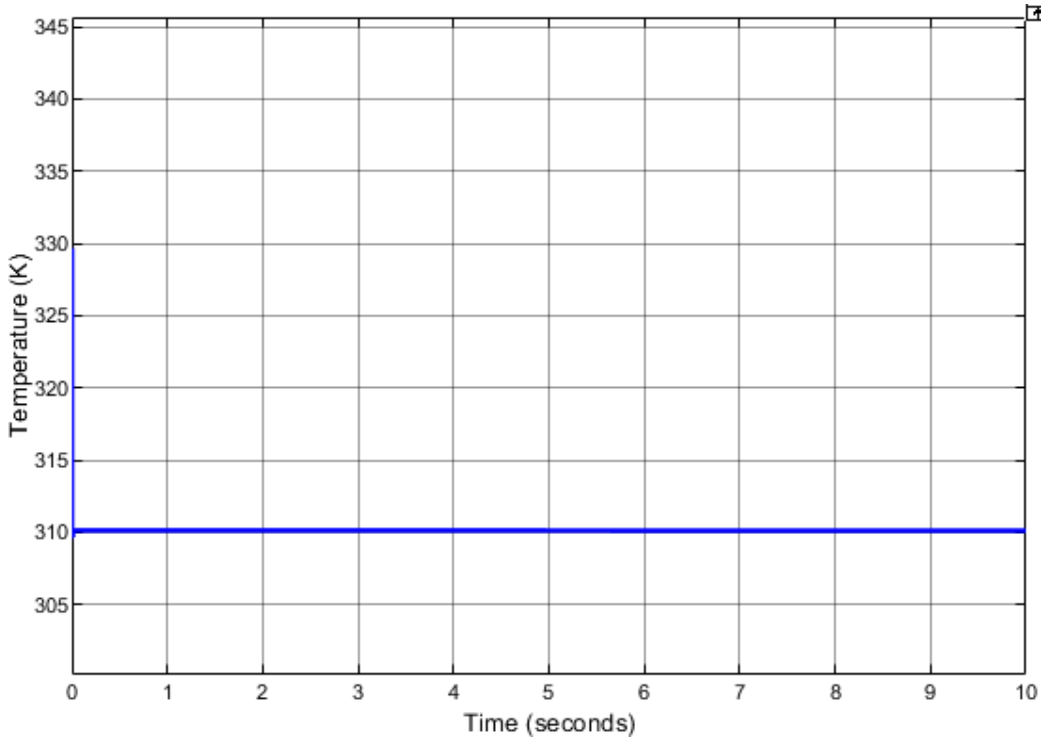

Figure III.19: PPR Temperature reding value.

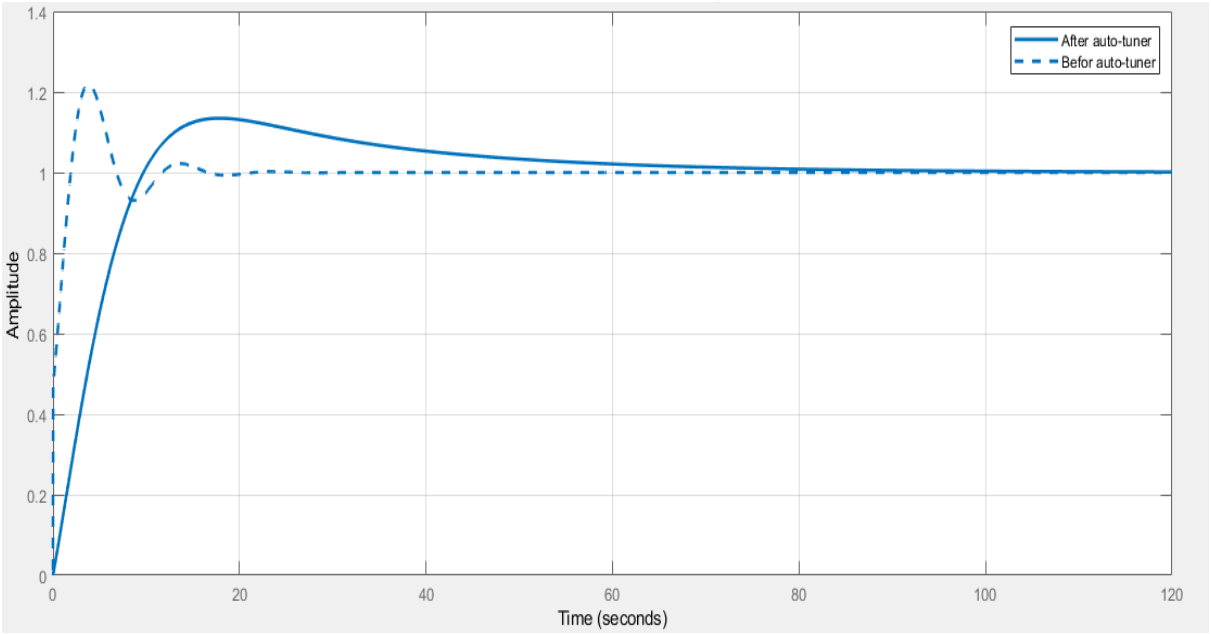

Figure III.20: Simulink PPR PID controller manual tuning & auto-tuner tool.

The (figure III.20) denotes the response of PID controller before and after using the Simulink auto-tuning tool, the fluctuations in the PID response cause of incorrect PID gains the K_P , K_I , K_D, high proportional gain (P) can cause overshooting, while insufficient integral gain (I) may lead to slow convergence, resulting in oscillations around the setpoint, improper derivative gain (D) might fail to dampen rapid changes, exacerbating instability.

Also, the insufflator system includes nonlinear components (mechanical valves, abdominal elastance /resistance) that complicate control. the use of MATLAB/Simulink PID auto-tuner to eliminate fluctuations by automatically optimizing PID gains to balance response speed and stability, accounting for system nonlinearities (abdominal resistance) through simulation, testing virtually to avoid physical hardware risks. MATLAB/Simulink auto-tuner tool provides a convenient way to optimize these parameters, allowing designers to improve system response based on specific performance goals [1.28].

III.4 Conclusion:

We explored and analyzed the carbon dioxide insufflation system using the MATLAB Simulink platform. The simulation produced stable and reliable results, demonstrating the system's effectiveness, stability, and feasibility for implementation. The tuned PID results show a smooth, rapid convergence to the setpoint without oscillations, demonstrating the effectiveness of model-based design. And ensures precise regulation of positive pressure delivered to the abdomen, maintaining stability without fluctuations.

General Conclusion

Through our study and deeper understanding of this project across the three chapters the medical aspect in the first chapter, the electronic aspect in the second chapter, and the practical implementation in the third chapter we obtained good results when testing this model in terms of the required temperature and pressure, as well as the effectiveness of the PID controller.This project successfully modeled and simulated a medical CO_2 insufflator system using MATLAB/Simulink, aimed at maintaining stable intra-abdominal pressure during laparoscopic surgeries. a PID controller was implemented to regulate pressure through a proportional pressure regulator, achieving stable and accurate results. The inclusion of a nonlinear abdominal model enhanced the realism of the simulation, allowing for better evaluation of system performance under different conditions.

The simulation proved the feasibility and effectiveness of using PID control in medical insufflation systems, offering a valuable tool for further research, development, and education. The project lays the groundwork for future improvements, including advanced control strategies and potential real-world implementation.

References

[1] A. Elsayed *et al.*, "MATLAB/Simulink Medical CO2 Insufflator Model with a Pressure PID Controller," *Middle East Conf. Biomed. Eng. MECBME*, vol. 2020-Octob, pp. 1–6, 2020, doi: 10.1109/MECBME47393.2020.9265117.

[2] I. Merdan, "Laparoscopic Entry: a Review of Techniques, Technologies, and Complications," *Basrah J. Surg.*, vol. 19, no. 1, pp. 10–23, 2013, doi: 10.33762/bsurg.2013.73613.

[3] J. Y. Cheong, A. Keshava, P. Witting, and C. J. Young, "Effects of intraoperative insufflation with warmed, humidified CO2 during abdominal surgery: A review," *Ann. Coloproctol.*, vol. 34, no. 3, pp. 125–137, 2018, doi: 10.3393/ac.2017.09.26.

[4] T. M. Atkinson, G. D. Giraud, B. M. Togioka, D. B. Jones, and J. E. Cigarroa, "Cardiovascular and Ventilatory Consequences of Laparoscopic Surgery," *Circulation*, vol. 135, no. 7, pp. 700–710, 2017, doi: 10.1161/CIRCULATIONAHA.116.023262.

[5] https://www.drdeeptiasthana.com/Dos-and-Don%27ts-After-Gynae-Laparoscopic-Surgery.php

[6] R. Sinha, A. K. Gurwara, and S. C. Gupta, "Laparoscopic surgery using spinal anesthesia," *J. Soc. Laparoendosc. Surg.*, vol. 12, no. 2, pp. 133–138, 2008.

[7] M. P. Frca and A. F. Frca, "Laparoscopic abdominal surgery," vol. 4, no. 4, pp. 107–110, 2004, doi: 10.1093/bjaceaccp/mkh032.

[8] https://trocarsupplies.com/blogs/news/everything-you-need-to-know-about-trocars

[9] https://metrodetroitcardiovascularassociates.com/services/transesophageal-echocardiography/

[10] https://www.turkcerrahi.com/en/general-surgery-articles/abdominal-wall-and hernias/quadrants-and-regions-of-abdomen/

[11] https://www.uptodate.com/contents/image?imageKey=PI/74006

[12] R. P. Borase, D. K. Maghade, S. Y. Sondkar, and S. N. Pawar, "A review of PID control, tuning methods and applications," *Int. J. Dyn. Control*, vol. 9, no. 2, pp. 818–

827, 2021, doi: 10.1007/s40435-020-00665-4.

[13] W. S. Al-dayyeni, “PID Control Perspective : Techniques and Uses,” pp. 1–8, 2025.

[14] B. Madhok, K. Nanayakkara, and K. Mahawar, “Safety considerations in laparoscopic surgery: A narrative review,” vol. 14, no. 1, pp. 1–17, 2022, doi: 10.4253/wjge.v14.i1.1.

[15] G. R. Umano, G. Delehaye, C. Noviello, and A. Papparella, “The ‘dark Side’ of Pneumoperitoneum and Laparoscopy,” *Minim. Invasive Surg.*, vol. 2021, 2021, doi: 10.1155/2021/5564745.

[16] J. E. Grabowski and M. A. Talamini, “Physiological effects of pneumoperitoneum,” *J. Gastrointest. Surg.*, vol. 13, no. 5, pp. 1009–1016, 2009, doi: 10.1007/s11605-008-0662-0.

[17] E. Yıldırım, K. S. C. Turhan, A. Güven, D. Gökmen, and M. Özcelik, “Factors Influencing Abdominal Compliance during CO2 Insufflation in Patients Undergoing Laparoscopic Abdominal Surgery,” *Reports*, vol. 7, no. 3, p. 52, 2024, doi: 10.3390/reports7030052.

[18] J. Y. Cheong *et al.*, “Randomized clinical trial of the effect of intraoperative humidified carbon dioxide insufflation in open laparotomy for colorectal resection,” *BJS open*, vol. 4, no. 1, pp. 45–58, 2020, doi: 10.1002/bjs5.50227.

[19] D. Wilhelm *et al.*, “Enhanced Visualization: From Intraoperative Tissue Differentiation to Augmented Reality,” *Visc. Med.*, vol. 34, no. 1, pp. 52–59, 2018, doi: 10.1159/000485940.

[20] H. Ren *et al.*, “Abdominal wall-lifting versus CO2 pneumoperitoneum in laparoscopy: A review and meta-analysis,” *Int. J. Clin. Exp. Med.*, vol. 7, no. 6, pp. 1558–1568, 2014.

[21] D. Göhler *et al.*, “Performance of intraoperative surgical smoke management technologies for laparoscopic surgery: A comparative in-vivo pig study,” *J. Aerosol Sci.*, vol. 177, no. June 2023, 2024, doi: 10.1016/j.jaerosci.2023.106309.

[22] W. L. Barrett and S. M. Garber, “Surgical smoke - A review of the literature. Is this just a lot of hot air?,” *Surg. Endosc. Other Interv. Tech.*, vol. 17, no. 6, pp. 979–987, 2003, doi: 10.1007/s00464-002-8584-5.

[23] D. Robertson *et al.*, “Escape of surgical smoke particles, comparing conventional and valveless trocar systems,” *Surg. Endosc.*, vol. 37, no. 11, pp. 8552–8561, 2023, doi: 10.1007/s00464-023-10444-9.

[24] Y. Lu, Q. Zou, B. Jiang, and Q. Li, “Perioperative outcomes and safety of valveless insufflation system in minimally invasive urological surgery: A systematic review and meta-analysis,” *Int. J. Surg.*, no. May, pp. 5763–5770, 2024, doi: 10.1097/js9.0000000000001634.

[25] S. Dormido, “Advanced PID Control - [Book Review],” no. March 2006, 2014, doi: 10.1109/MCS.2006.1580160.

[26] T. Hägglund and K. J. Åström, “Automatic tuning of PID controllers,” *Control Syst. Handb. Control Syst. Adv. Methods, Second Ed.*, pp. 759–778, 2010, doi: 10.1201/b10384.

[27] V. Der Zalm, “Tuning of PID-type controllers,” vol. 2004, no. 2004, 2025.

[28] J. Unde, “Simulating ‘Electronic Pressure Regulator’ using MATLAB Simulink,” *Int. Res. J. Eng. Technol.*, no. December, 2008, [Online]. Available: www.irjet.net

الملخص

هدفنا هو تطوير نموذج محاكاة لجهاز نفخ ثاني أكسيد الكربون(CO_2) ، وهو جهاز طبي يُستخدم في العمليات الجراحية بالمنظار (الجراحة طفيفة التوغل) لنفخ التجويف البطني بغاز ثاني أكسيد الكربون .(CO_2) يوفّر هذا فراغًا عمليًا للجراحين من خلال الحفاظ على ضغط داخل البطن (IAP) مستقر. نستخدم وحدة التحكم PID مع أدوات الضبط التلقائي (automatic-tuning) لتحقيق استجابة سريعة، واستقرار في الأداء، وأقل تجاوز ممكن.

الكلمات المفتاحية: درجة الحرارة، الضغط، ، جراحة بالمنظار

Abstract

Our goal is to develop a simulation model of a CO_2 insufflator, a medical device used in laparoscopic (minimally invasive) surgeries to inflate the abdominal cavity with carbon dioxide (CO_2) gas. This creates a working space for surgeons by maintaining a stable intra-abdominal pressure (IAP). Using the PID controller with the automatic-tuning optimization tools to ensure fast response, stability, and minimal overshoot.

Keywords: Temperature, Pressure, Laparoscopic surgery.

Résumé

Notre objectif est de développer un modèle de simulation d'un insufflateur de CO_2, un dispositif médical utilisé lors des chirurgies laparoscopiques (chirurgies mini-invasives) pour gonfler la cavité abdominale avec du dioxyde de carbone (CO_2). Cela permet de créer un espace de travail pour les chirurgiens en maintenant une pression intra-abdominale (PIA) stable. Nous utilisons un régulateur PID avec des outils d'optimisation à réglage automatique afin de garantir une réponse rapide, une bonne stabilité et un dépassement minimal

Mots-clés : Température, Pression, Laparoscopique chirurgie.